JEM–X Performance and Calibration Status Report

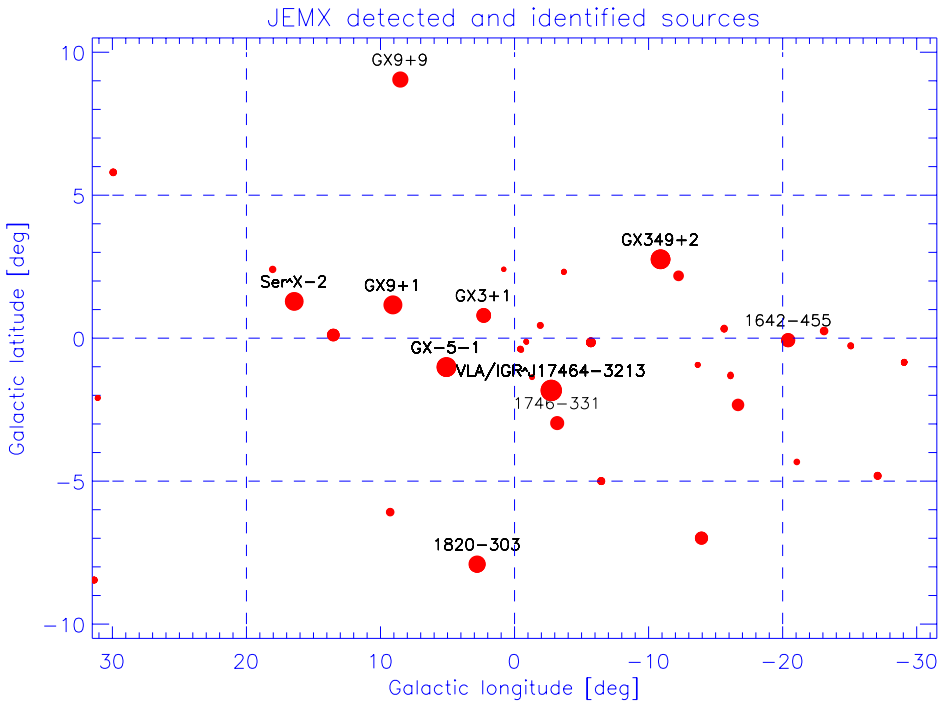

DSRI Project JEM–X

Document No. IN–PL–JEM–0018

Issue 1, Rev. 0

May 6, 2003

Picture on front page: Identified sources found by JEM-X during the Galactic Centre Deep Exposure. The brightest sources are marked by name. The source marked VLA/IGR J17464-3213 is the radio counterpart suggested in IAUC # 8105 to the INTEGRAL source IGR J17464-3213. The angular separation of the radio couterpart and the "nominal" INTEGRAL source is about 2 arcminutes. The JEM-X data strongly favors the radio position as the position of the X-ray source

JEM–X
Performance and Calibration Status Report

IN–PL–0018

Issue 1, Rev. 0

DSRI Project JEM–X

Prepared by:
Niels Lund, Niels J. Westergaard, Carl Budtz-Jørgensen,
Carol-Anne Oxborrow, Søren Brandt, Jerome Chevenez
and Ib Lundgård Rasmusssen
DSRI

Date: May 6, 2003

Approved by: Date:

Approved by: Date:

DSRI

Revision Notice

Document Revision History			
Issue	**Rev.**	**Date**	**Changes**
1	0	May 6, 2003	Initial Release

List of Acronyms

CSSW	Common Services Software
DFEE	Digital Front-End Electronics
DXB	Diffuse X-ray Background
EW	Equivalent Width
FOV	Field of View
FWHM	Full Width at Half Maximum
IASW	Instrument Application Software
IREM	Integral Radiation Monitor
OEM	On Event Message
PSF	Point Spread Function
SPR	Science Performance Report

Contents

1 Introduction

This report summarizes the results obtained during the initial seven months of JEM-X operations on board INTEGRAL. The instruments have now been tuned to good operational conditions, and although these differs from what was originally planned, the actual performance is close to the pre-launch expectations.

The most significant anomaly encountered during the commissioning was the erosion of the microstrip electrodes resulting in a gradual loss of sensitivity. By lowering the operating voltage and thereby the gain of the detectors we have succeeded in reducing the damage rate to a level where the survival of the instruments for a five year period seems to be assured.

The calibration data, primarily those from the observations of the Crab pulsar and nebula in February 2003, are of exellent quality and permits to determine the instruments characteristics adequately for the support of a scientific analysis.

Table 1: **JEM-X Characteristics according to the AO-1 Documentation**

Sensitive detector area (total for 2 units)	1000 cm^2
Energy range	3 - 35 keV
Field of View (diameter)	4.8° Fully illuminated 7.5° Half response* 13.2° Zero response
Energy resolution	$\Delta E_{FWHM}/E = 0.40/\sqrt{E[\mathrm{keV}]}$
Angular resolution (FWHM)	3 arcmin
Point source location	30 arcsec (for a 10σ) source
Narrow Line sensitivity (isolated source on-axis)	1.7×10^{-5} photons $s^{-1}\,cm^{-2}$ @ 6 keV 5.0×10^{-5} photons $s^{-1}\,cm^{-2}$ @ 30 keV for a 3σ line detection in 10^6s
Continuum sensitivity (isolated source on-axis)	1.3×10^{-5} photons $s^{-1}\,cm^{-2}\,keV^{-1}$ @ 6 keV 8.0×10^{-6} photons $s^{-1}\,cm^{-2}$ @ 30 keV for a 3σ continuum detection in 10^6s
Timing resolution	122 μ s

* At this angle the sensitivity is reduced by a factor 2 relative to the on-axis sensitivity.

2 JEM-X Performance

2.1 Energy Range and Resolution

The gas gain decrease has modified the low energy thresholds of the detectors. Fig. 1 compares the empty field energy spectrum obtained before the gain change (left) with the one measured after the gain change (right). There is a clear loss of events in the low energy part of the latter spectrum. A more detailed analysis have shown that the 50% efficiency level is now reached at 4.2 keV, just after launch it was at 3.5 keV. The upper energy limit of JEM-X has not been affected by the change in gas gain since this limit is determined by the gradually diminishing absorbtion cross section of the Xenon gas above 25 keV and by the sharp K-edge at 35 keV. In order to economize on the telemetry usage the detectors are presently operated with an upper threshold set by software around 50 keV.

The detector energy resolution is primarily determined by the number of free electrons liberated during the X-ray absorbtion process and therefore is not significantly affected by the reduction of the gas gain. The energy resolution of the Xe Kα fluorescence line which is detected all over the sensitive area is still 9.0% in both JEM-X1 and JEM-X2.

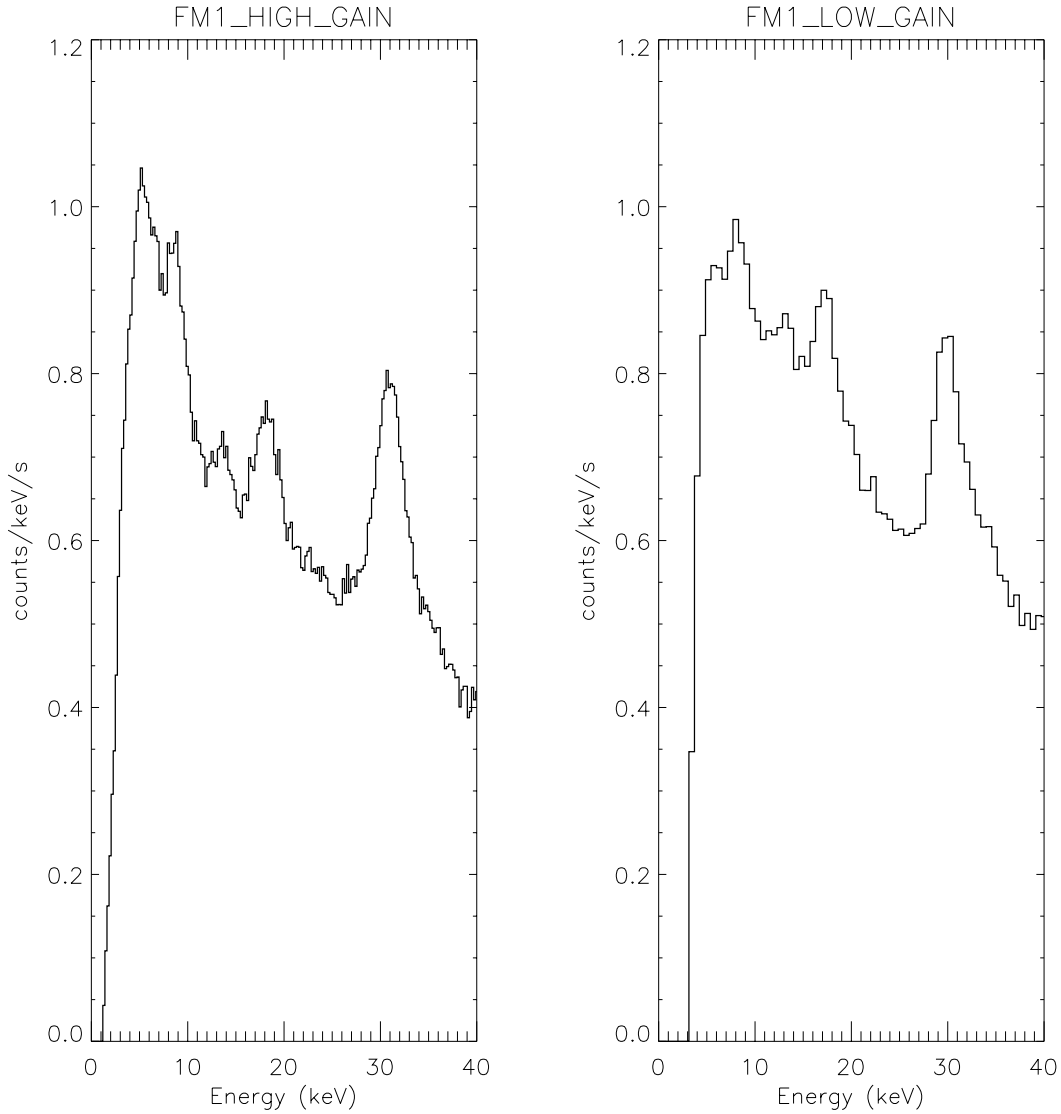

Figure 1: *Empty field background spectrum measured with the nominal detector gain of 1500 (left) compared to the background spectrum obtained with the reduced gain of 600 (right).*

2.2 Timing Stability and resolution

The extended observations of the Crab pulsar have permitted to perform and end-to-end test of the timing properties of the JEM-X data. It is noted that the timing properties of both JEM-X units are found to be identical. As illustrated in Figure 2 the steady slowing down of the Crab pulsar (36 ns/day) can be followed hour by hour by JEM-X. Note that the solid line in the figure is not a fit to the data points but the Crab pulsar radio ephemeris as published by the Jodrell Bank Observatory. This demonstrates that the timing of the JEM-X data is stable enough to track the period of the Crab pulsar with an accuracy of a few nanoseconds or better over several days.

There remains an uncertainty of about 1 ms regarding the absolute timing of the data. JEM-X (and also XMM) finds that the main peak in the X-ray pulsar signal leads the main peak in the radio signal by about 1.5 ms (see Figure 3). RXTE, for which pulsar timing is one of the primary activities, finds that the lead is only 0.4 ms. The absolute time calibration performed on the ground in ESTEC showed an offset of JEM-X timing of 0.18 ms relative to the onboard clock. This correction has been included in the analysis above. The analysis used the onboard time relation and orbit information provided by MOC. There seems to be glitches of at least 100 micro seconds associated with ground station handovers, but does not seem to significantly affect the analysis.

Observations separated by 20 days were used to determine the absolute timing of the arrival of the main Crab pulse. The absolute timing difference was found to be less than 0.1 ms, demonstrating a clock stability of the combined system of the JEM-X clock, Integral onboard clock, and the ground segment better than 10E-9. The timing resolution of JEM-X is 122 micro-seconds, in the sense that each photon is determined to lie in a bin of that width. However, as the analysis shows, the phase of the timing bins is well determined with a much better accuracy, consistent with the on-ground timing test results showing that the bin phase is accurate to within a few micro-seconds.

The cause of the offset of 1.1 ms in the absolute timing relative to the RXTE result is presently not known.

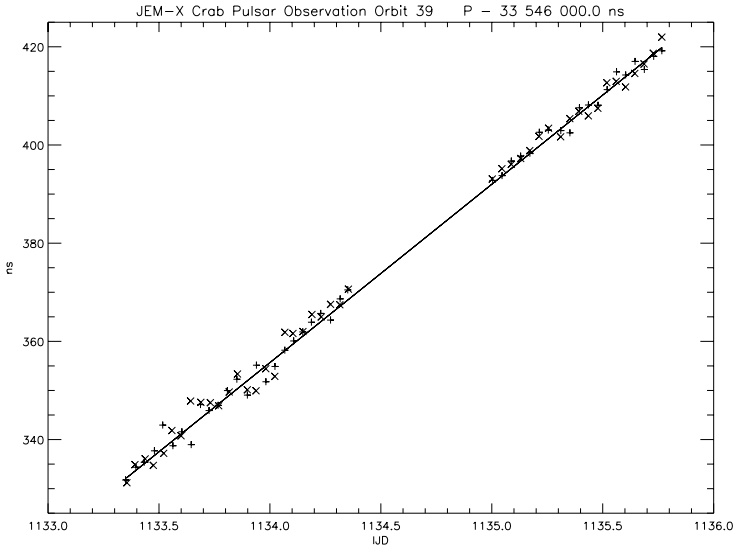

Figure 2: *Determination of the Crab pulsar period independently by JEM-X1 and JEM-X2 during orbit 39 using data intervals of 1 hour. The solid line is the expected period from the Jodrell Bank Observatory radio ephemeris*

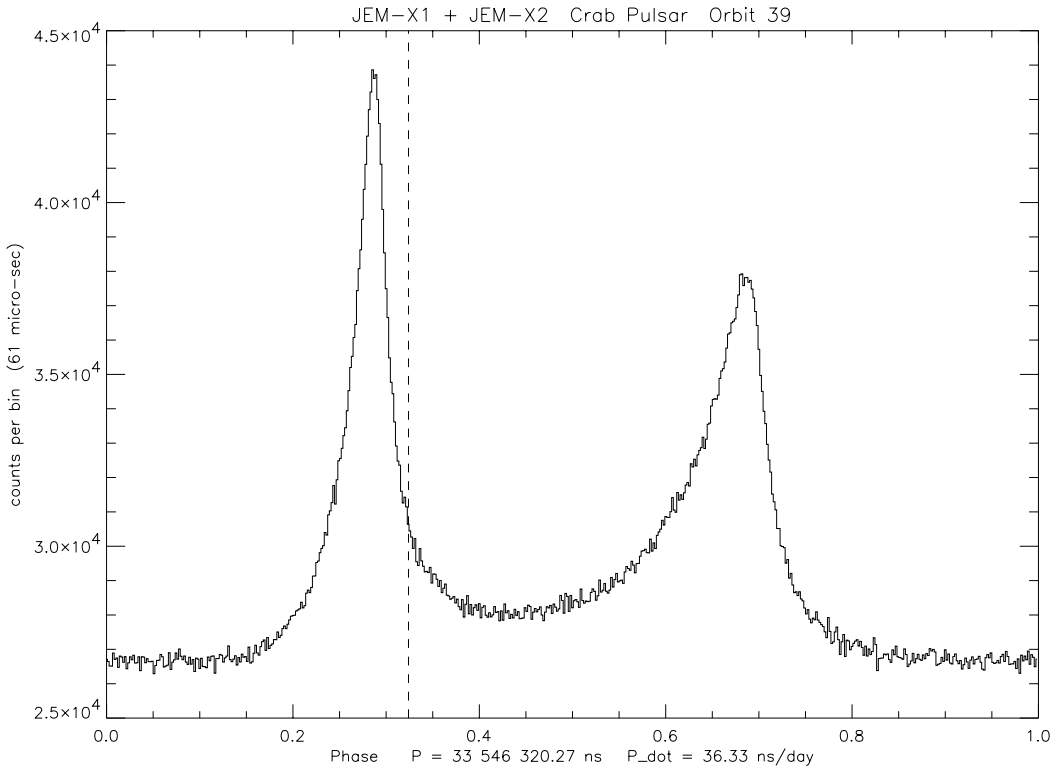

Figure 3: *The pulse profile of the Crab pulsar using 16 million photons observed during orbit 39 with JEM-X1 and JEM-X2. The folding was done using the predicted period and period derivative. The pulse was sampled with a bin size of 61 micro-seconds, half the size of the intrinsic time resolution of JEM-X. The narrow main peak demonstrates the stability of the end-to-end timing system. The vertical line indicates the position of the radio peak. The X-ray peak leads the radio with 1.51 ms, or about 1 ms more than expected from XTE observations*

2.3 Source positioning uncertainty

The source position determination consists of two parts:

- Instrument boresight with respect to star-tracker direction
- Intrinsic instrument position determination

The early Cyg X-1 observations were used to determine the mis-alignment matrix in the package DAL3AUX.

The intrinsic position determination is based on the corrected detector positions of the events.

A study of the results of the standard (ISSW) software source position accuracy has been made from the Crab calibration observations and the result is shown in Fig. 5. The systematic deviation of 19 arcsec could be reduced by updating the mis-alignment matrix (work in progress).

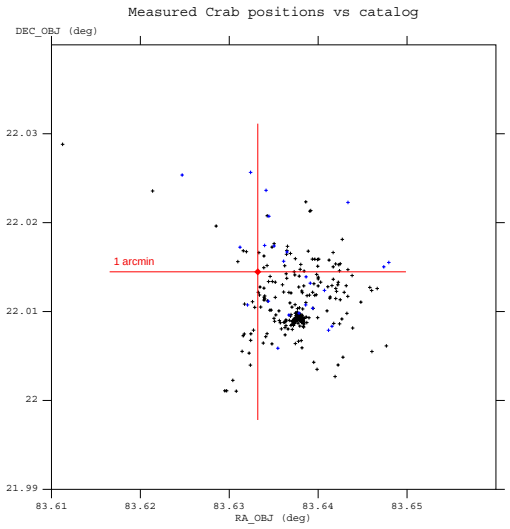

Figure 4: *Distribution of the Crab position in 244 pointings. The large cross shows the SIMBAD catalog position. There is a distance of 19 arcsec between this and the average position. The standard deviation of position with respect to the average position is 14 arcsec. (Courtesy P. Kretschmar)*

When the Crab is observed away from the pointing axis the position accuracy drops because of weaker signal and the parallax effect. Fig. 5 shows how much better the position is determined when the source

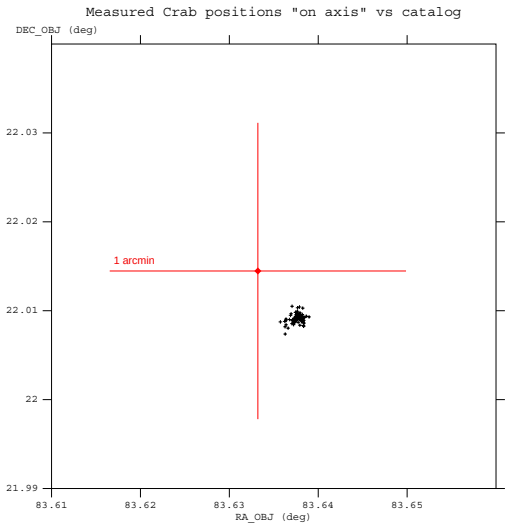

Figure 5: *Distribution of the Crab position from pointings where it is found close to the pointing axis. The large cross shows the catalog position for the Crab pulsar. (Courtesy P. Kretschmar)*

is almost on-axis.

Next generation imaging software will probably reduce the scatter (work in progress). The intrinsic systematic errors corresponding to different positions within the field-of-view. For sources lying less than 4 degrees off axis the systematic errors are less than 10 arcseconds, between 4 and 5 degrees the systematic errors are more difficult to determine because of the rapidly falling efficiency of the instrument, but they appear to increase to about 20 arcseconds at 5 degrees. Some of this effect is due to parallax effects and these may be compensated for in the analysis. Beyond 5 degrees we do not recommend to use JEM-X for source positioning.

The Crab observations also provided an opportunity to demonstrate the good stability and the statistical precision of the source location with JEM-X. It is known from several X-ray imaging studies of the Crab complex that the pulsar is offset in position by 10 to 20 arcseconds from the centroid of the nebular emission. We have made multiple position determinations for the total Crab signal, phase resoved according to the pulsar period. And, as shown in figure 6 the derived position actually oscillates by about 12 arcseconds during the pulsar period. The statistical uncertainty on the individual positions is about 1 arcsecond due to the excellent count statistics in this observation.

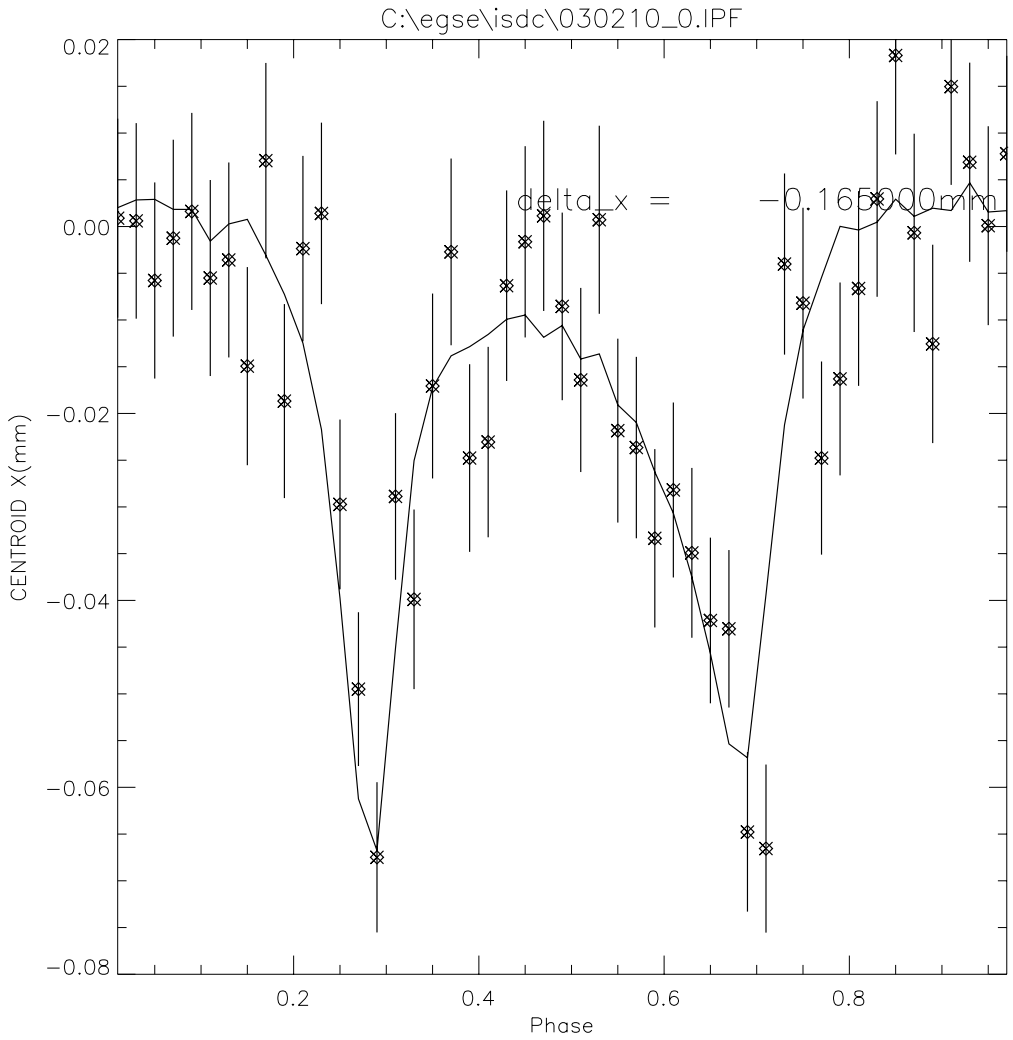

Figure 6: *Phase resolved determinations of the centroid of emission from the Crab complex (pulsar + nebula). The separation of the pulsar position from the centroid of the nebular emission results in a "wiggling" of the position in synchronism with the pulsar signal.*

2.4 Background

The JEM-X background has been derived from from a number of empty field observations. The background rate is about 20 cts/s in the 4 to 35 keV range when INTEGRAL is outside the radiation belts. This is about a factor two higher than predicted before launch.

Fig. 1 illustrates the background energy spectra measured under these conditions. The lines seen here were also observed during the ground calibrations and stem from Cu, Mo and Xe fluorescence and a weak U contamination of the Be window.

The radial variation in the background across the detector is shown in figure 7. The increase of the background towards the edge of the detector is noticeable.

Table 2 compares the pre-launch predictions for the background count rates with the actual values observed in flight. The count rate data for the Crab (pulsar + nebula) are also shown for reference.

Table 2: **JEM-X predicted and actual‡ countrates**

Interval (keV)	Source (counts/s)		DXB* (counts/s)		CR† (counts/s)		Total bkg (counts/s)	
	predict	actual	predict	actual	predict	actual	predict	actual
3(4) - 10	147	(83)	4.1	(3.0)	0.8	(3.1)	4.9	(6.1)
10 - 20	37	27	2.4	1.8	1.1	5.1	3.5	6.9
20 - 35	7.4	5.4	0.6	.5	2.3	6.5	2.9	7.0
Tot: 3(4) - 35	191	(115)	7.1	(5.3)	4.2	(14.7)	11.3	(20.0)

‡ Due to the change of gas gain the actual count rates (in parentheses) refers to a slightly different energy range than used for the predictions.
The actual count rates are also affected by the deadtime and dead anode losses.
These effects were not considered in the pre-launch calculations

* *Diffuse X-ray background*

† *Cosmic Ray (i.e. charged particles and gammas)*

We see two possible causes for the strong increase in the cosmic ray induced background. One could be that our rejection of cosmic ray particles traversing the detector is less effective than predicted. The second is that the background of hard X- and gamma rays produced by the cosmic rays in the surrounding payload elements is significantly higher than expected. We believe the second cause to be the most important one. The increase of the background towards the edge of the detector is rather natural if the background arises from photons generated in material around the JEM-X detectors; such an increase would be more difficult to understand if the background was caused by direct traversals of the detector volume by cosmic rays.

However, we have realized that the background count rate in the energy range above 8 keV did increase in connection with our latest change of on-board event rejection criteria. This is noticeable when comparing the left and right panel of figure 7. The change was very successfull in improving the instrument efficiency below 8 keV, but apparently this was achieved at the expense of the high energy rejection efficiency. We believe we can modify the on-board logic to achieve simultaneously high efficiency in the low and high energy ranges, but this will require patching of the on board software. We are currently working to quantify the sensitivity gain we may achieve through such a patch.

When the Sun is active and the satellite attitude is such that the Sun illuminates the JEM-X masks the background in JEM-X may temporarily increase substantially. These situations are, however, relatively rare and only few observations are affected by this problem. It is believed that X-rays from the Sun are

scattered into the detector by the mask and its support structure.

So far there has been no indication of a significant long term increase in the background due to radiation activation of the detectors or their surroundings. The monitoring of the background orbital and pointing dependencies will be continued.

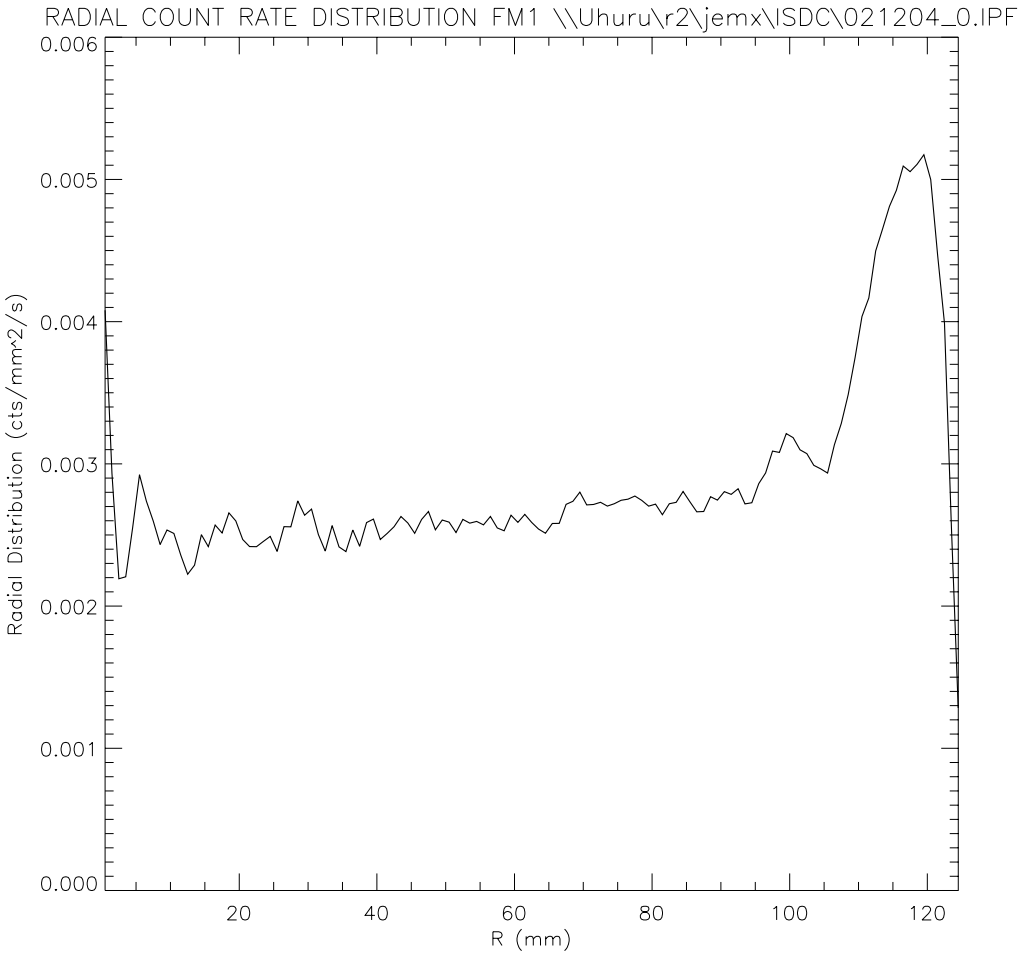

Figure 7: *Radial background countrate distribution for JEM–X 1.*

2.5 Source sensitivity

Most of the science data from JEM-X 2 have been analyzed with off-line imaging tools as a preparation for the next generation image analysis. Here we only compare the source finding sensitivity for the special case of the quasar 3C273 with the AO-1 claims in Fig. 8 where the thick line is the detection limit based on simulations where the source is on-axis and there are no other sources in the FOV. The thick dashed line show the same result where a source of Crab intensity is placed 3 deg off-axis.

We are preparing an analysis involving a large set of sources observed during the Galactic Centre Deep Exposure and the Galactic Plane Scans in order to plot their detection levels on a similar plot.

The current standard ISSW executables for imaging do not quite reach this level of sensitivity.

As an example the observation (SWID=001900400010, see Fig. 4.4) has been used with JEM-X2 data. The source EXO 2030+275 is the most significant source here. With the ISSW software (OSA release) the countrate is 1.6 counts/s (5-27 keV). The Crab count rate in the same energy interval is about 80 counts/s so the EXO 2030+275 strength is 20 mCrab. The detection significance is 23.8 i.e. well above the value recommended for a safe identification - about 14.

2.5.1 Continuum sensitivity

See comments in section 4.4 where the extracted source spectrum is shown.

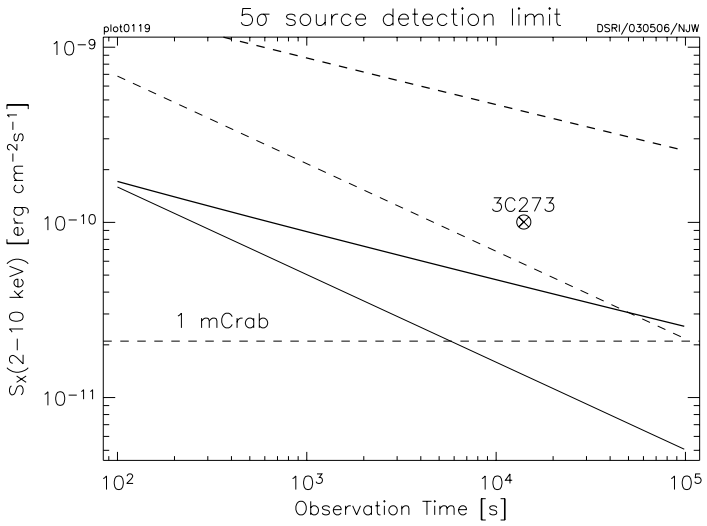

Figure 8: *JEM-X five sigma source sensitivity plot (from the AO-1 documentation) with actual JEM-X source detections overplotted. Only candidates identified with sources in the DSRI X-ray catalog (1500 entries) are shown.*

2.6 JEM–X Engineering Performance

The JEM-X engineering performance is nominal, except for the long term gain increase described below.

The gain variation during the first hours after HV activation is as expected In each orbit at the beginning of the observations the gain is initially about 20% higher the desired value. The desired level is reached in about 2 hours, and the internal calibration sources allows fully correct the data on ground.

Unexpectedly, the gain of the microstrip detectors has shown a gradual rise over time. The gain of JEM-X2 has increased by about one percent every four days. Figure 9 shows this overall trend. After 200 days and a gain increase exceeding 25 percent it was decided to lower the HV setting by one step, corresponding to 10 Volts. This measure reduced the gain by 12 percent (slightly less than expected) and adjusted the gain to a level comparable to that seen during the Crab calibration. However, the increase continues and further high voltage adjustments are planned to keep the gain close to the Crab reference. The reason for the increase in gain as function of time is unknown, but the gain variations are tracked by the onboard calibration sources and the Xenon flourescense peak in the background data.

The thermal environment is stable. The detector temperature varies with a few degrees depending on the orientation of the spacecraft. The detector gain increases by about one percent per degree of increase of the detector temperature. This effect is similar to what was observed during the thermal vaccum test.

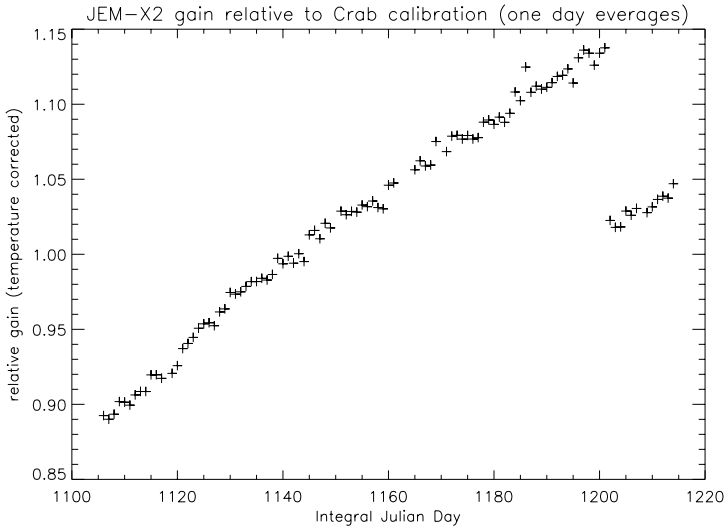

Figure 9: *Average relative gain for JEM-X2 as function of time. The data are normalized to the average gain during the Crab calibration starting at IJD=1133. Data closer than 0.5 day after the HV activation have been excluded. The gain is corrected for temperature variations of the detector. The 12 percent drop in gain at IJD=1202 corresponds to the time of reducing the high voltage by 10 Volts.*

2.7 Microstrip degradation in Space Environment

A serious anomaly was detected after one week of operation, namely a continuing loss of sensitivity of the microstrip detectors. Each detector contains 256 individual anode strips - 10 micron wide chromium strips on a glass substrate. Within the first week about 15 such anodes in each detector had ceased to function. Electrical discharges between the anode and cathode strips are suspected to disrupt the anode strip at its root so the remaining anode strip becomes a free floating electrode with the same electrical potential as the surrounding cathode areas. The discharges are suspected to be caused by the traversal (and maybe nuclear interactions) of heavily ionizing cosmic ray nuclei.

After recognition of the this anomaly the operating voltage of the microstrip detector was lowered from about 900 V to about 820 V, and later to 800 V. This reduction has reduced the damage rate from about 15 anodes per week to about 1 anode per month per instrument. At this rate the instruments will retain mor than half their original sensitivity after 5 years of operation.

The microstrip status is described in more detail in the Technical Note attached as an appendix to this report. Since the writing of the report we have seen one more anode loss in JEM-X2 - consistent with the rate of about one anode lost per month. A map of the JEM-X2 detector with indication of the suspect anodes is shown below.

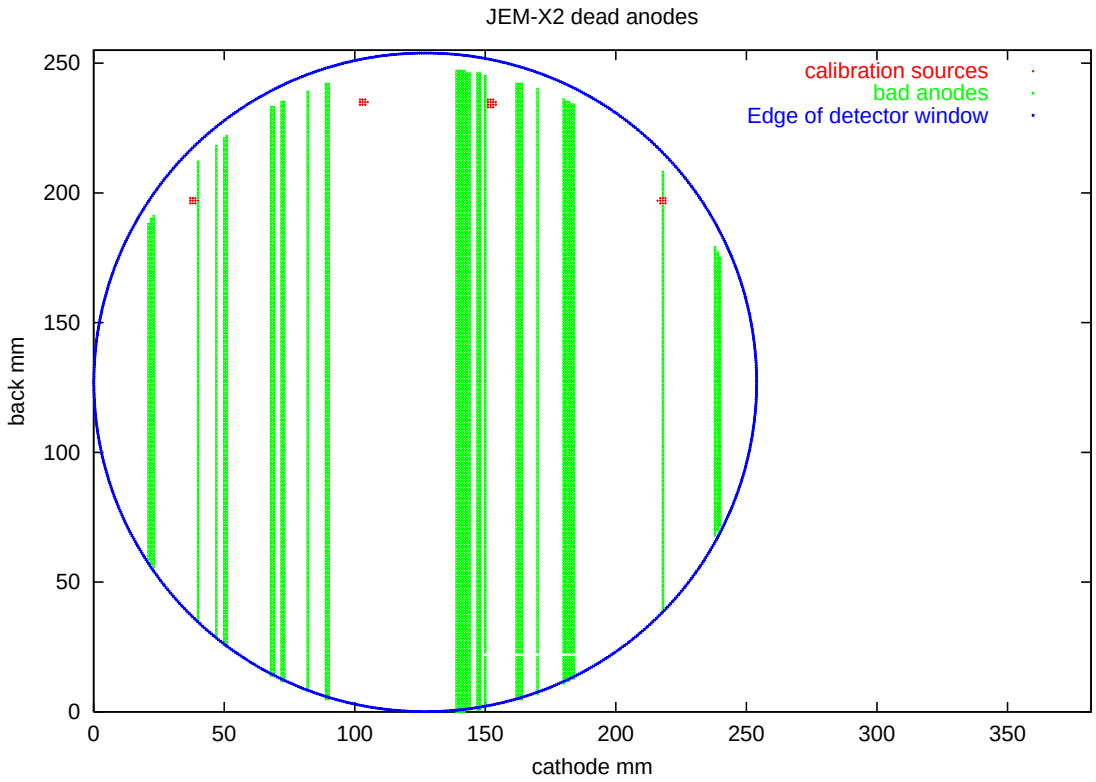

Figure 10: *Map of the JEM-X2 detector with the dead anodes marked in green.*

3 3 Calibration Status

3.1 Spectral Response

The spectral response of JEM-X is critical dependent on the correct adjustment of the on-board background rejection criteria. In figure 11 and figure 12 are shown the data from the last on-axis Crab pointing, made after the final JEM-X parameter update. The purpose af the last update, made only a few days before the conclusion of the Crab calibrations was precisely to recover a number of good events which had, until then, been rejected by the on board software.

The gradual loss of sensitivity at low energies are caused both by absorbtion of photons in the detector window (0.25 mm Beryllium) and by electronic threshold effects, which have become more marked after we were forced to reduce the gas gain in the detectors.

We are, however, quite satisfied with the result. We conclude that the significant reduction in gas gain (from about 1500 to about 600) have only led to a marginal increase in our effective low enrgy threshold, this has moved up from 3.5 to 4.2 keV.

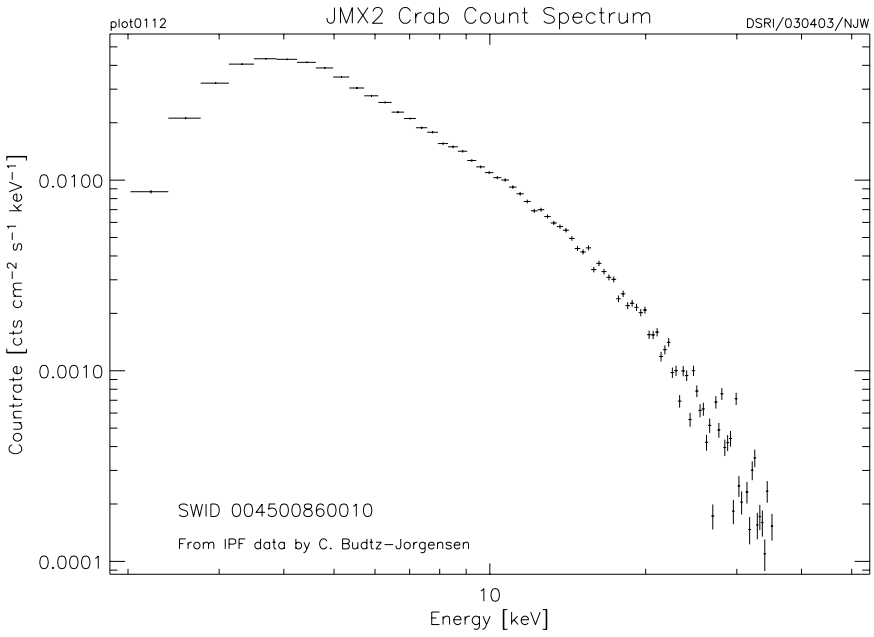

Figure 11: *The final observed Crab photon spectrum (after parameter adjustment)*

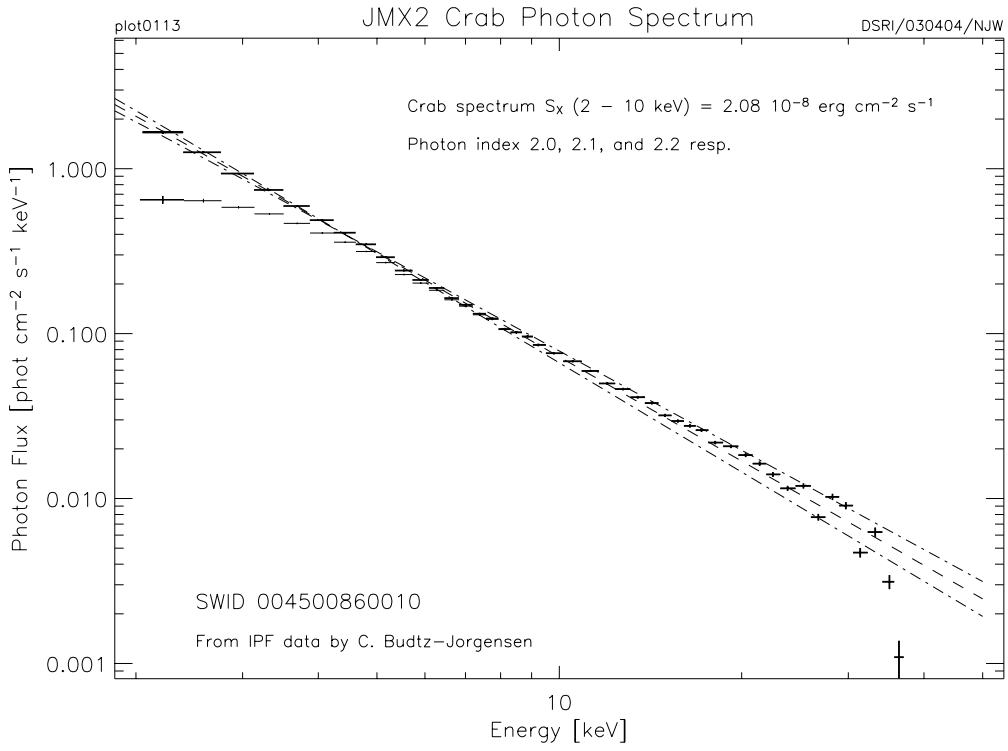

Figure 12: *Deconvolved Crab spectrum corresponding to figure 11. Three simple power law spectra are overplotted for comparison.*

3.2 Photon localization

The reduction of the operating voltage and the resultant decrease in the detector gas gain has lead to some degradation of the detector position resolution. The position resolution, however, is still adequate to resolve the hole pattern of the JEM-X coded mask.

Fig. 13 displays the telescope 2D Point Spread Function derived from an observation of Cyg X-1. The detector coordinates (DETX, DETY) are given in mm. (1 mm corresponds to 0.99 arcmin in the photon arrival direction). The PSF is well represented by a 2D Gaussian function with standard deviations of 1.44 arcminutes for both sigma_x and sigma_y. It should be noted that the width of the distribution is dominated by the dimension of the holes in the mask. Over most of the energy range the localization of the photons is much better than the dimension of the mask holes.

We have analyzed the JEM-X PSF as function of X-ray energy. Fig. 14 displays the energy dependence of the widths sigma_x and sigma_y. The increase of the widths towards lower energies reflects the decrease of the detector position resolutions as the signal-to-electronic noise ratio decreases. We stress that the detector position resolution over the whole 3-35 keV band is sufficient to achieve useful imaging results.

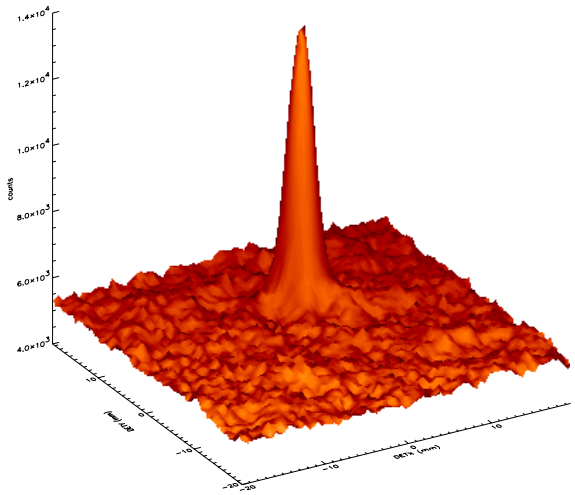

Figure 13: *Derived point spread function of Cyg X-1 signal derived from an on-axis observation in JEM–X 1.*

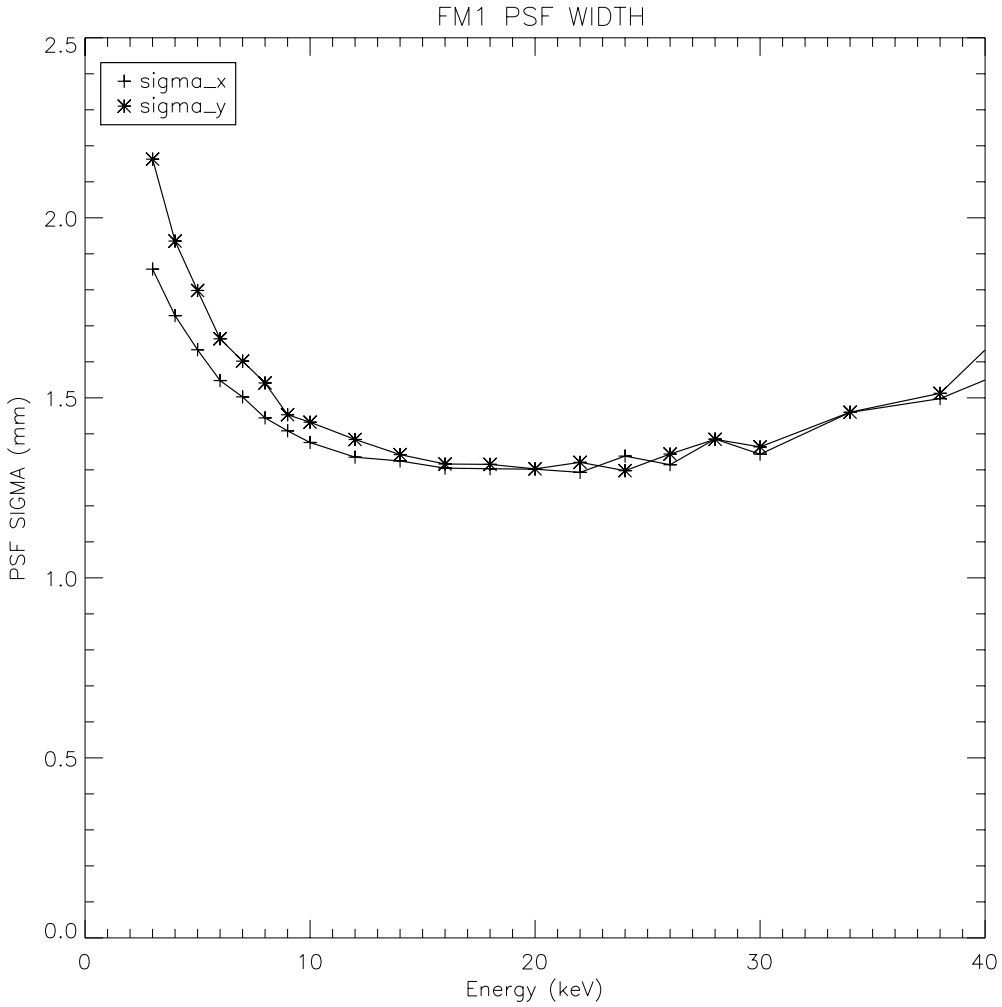

Figure 14: *The width of the JEM-X point spread function as a function of energy.*

3.3 Misalignment

As illustrated in section 2.3 there is still missing a small correction for the mis-alignment between star-tracker and instrument. For strong sources the statistical accuracy is much better than the remaining systematic error. Work is ongoing to update the misalignment matrix in the DAL3AUX library.

3.4 Timing offset

The Crab calibration has shown that the JEM-X absolute timing offset appears to be about 1 ms (see section 2.2). The source of this offset (if real) is to be found outside of JEM-X itself, as the performance of JEM-X is such that we must consider the pre-launch time calibrations against the onboard clock as valid. Therefore the 1 ms offset has to be found in the relation of the onboard time to terrestial time (done by MOC and distributed by ISDC), or in the analysis software used to convert the terrestial time to a barycentric reference frame for the arrival of the Crab pulsar photons.

3.5 Effective area and effective field-of-view

The effective area of the JEM-X detectors is nominally the area of the beryllium window (491 cm^2) minus the 6% covered by the collimator footprint. At present there are 42 suspect anodes in JEM-X2 removing another 16 % of the area. Finally, the uneven distribution of the background makes it advantageous from to remove a further 15 % of the detector area to achieve an optimal signal to noise ratio for the data. All in all the effective area of the JEM-X detectors are therefore reduced to about 330 cm^2. Taking into account the 25% transmission mask an on-axis source will illuminate about 82 cm^2.

The collimator and the mask limits the JEM-X field of view. We have found that although the zero transission angle of the collimator nominally is 6.6° off axis, in practice the transmission of the collimator beyond an off axis angle of 5° is so low that only the very brightest sources can be observed at larger angles.

3.6 Deadtime

The deadtime of the JEM-X detector has been determined to be less than 12 percent during normal observations without any strong sources in the field of view. For observations of stronger sources the deadtime increases by one percent for each additional 55 counts/sec in accepted X-ray events. This means that the deadtime for an observation of the Crab on-axis increases by about 2 percent.

The deadtime is derived from the housekeeping data providing information about the number of triggers being handled in the individual branches of the onboard processing. See figure 15 Detailed knowledge about the deadtimes introduced in each channel enables the calculation of the total deadtime with an 8 second time resolution. Calculation of the deadtime with finer time resolution than 8 seconds, as required during short but very intense X-ray bursts, is also possible as the background can be considered constant and the differential deadtime calculated from the increase in accepted events.

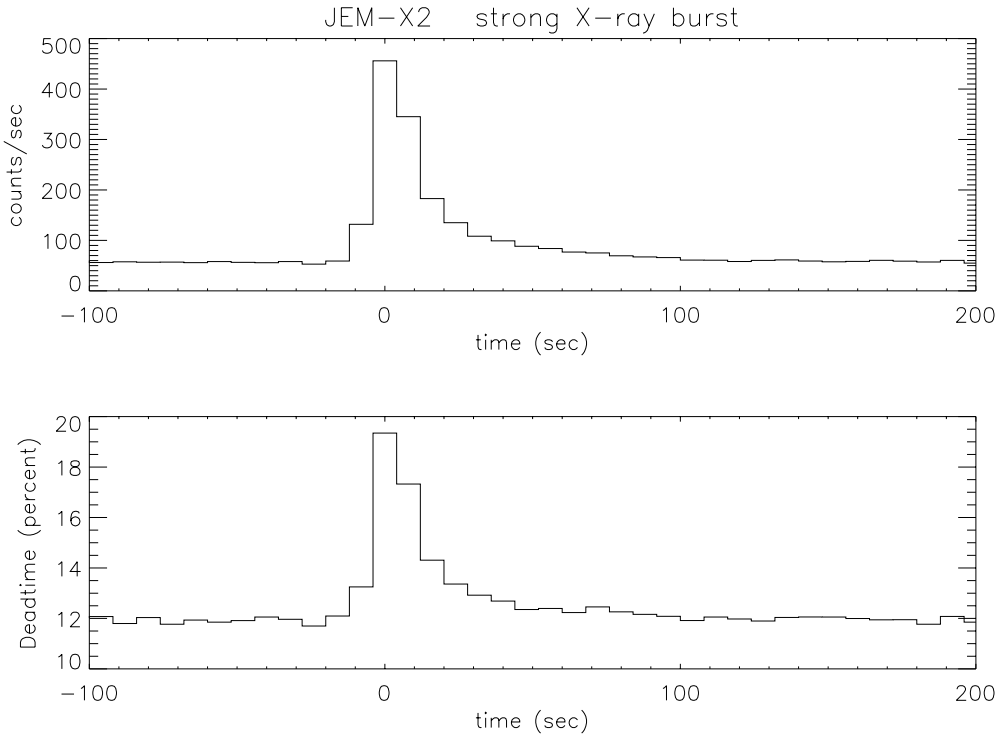

Figure 15: *Example of rapidly varying deadtime during a very strong (5 Crab) X-ray burst. The upper panel shows the rate of accepted X-ray events. The lower panel shows the deadtime calculated from the housekeeping data. The deadtime corrected light curve can then be plotted using these two curves*

3.7 Future Work

4 JEM-X software at ISDC

4.1 Gain correction

The gain calibration software installed at ISDC has matured considerably since the launch. Some major changes have been made to the software to reflect some unexpected realities of the calibration spectra.

Originally the Ni fluorescence lines at 8 KeV were supposed to be used in tandem with the Cd-109 (or Fe-55) lines at 22 KeV to provide the linear gain conversion factors for each of the four anode segments. However it became apparent immediately after switch on that these peaks were far too weak to be detected reliably by the Automatic Calibration and Correction (ACC) software—with the consequence that very erratic gain conversion factors very produced early in the mission.

This problem has been corrected by using the Cd/Fe lines in conjunction with known gain offset (nominally and actually zero) channel for each detector. The offset channels are monitored every revolution by the onboard electronic calibration (ECAL) procedure, part of which was expanded prior to launch to include offset (null-pulse) monitoring. This means that we are now in a position to update the zero-energy offset channels if these should change or drift. No such change has yet been seen in the amplifier-ADC behaviour of either unit.

While the time-varying component of the energy gain factor was already corrected for in the ISDC software at launch, the spatial gain variation correction has been added relatively recently, but appears to work well. This part of the spatial gain variation was determined by prelaunch calibration at Ferrara, the results of which are stored as two tables JMX1-SPAG-MOD and JMX2-SPAG-MOD in the instrument model tables JMX[1,2]-IMOD-GRP.

There is one final adjustment that must be incorporated into the ISDC software, and that involves a spatial gain variation table for mapping the effect of dead anodes. This table is still being constructed from off-line analysis of spectra for individual strips of pixels all with the same RAWX value. Figure 4.1 shows how gain resolution is improved first by performing the time and spatial gain corrections, and then by correcting for the individual anodes areas. These results were produced by an offline analysis on JEM-X2 data. While it is clear that some improvement in resolution is to be gained by doing the anode-by-anode correction, we can also see that the currently implemented corrections come a very long way to achieving the desired energy resolution.

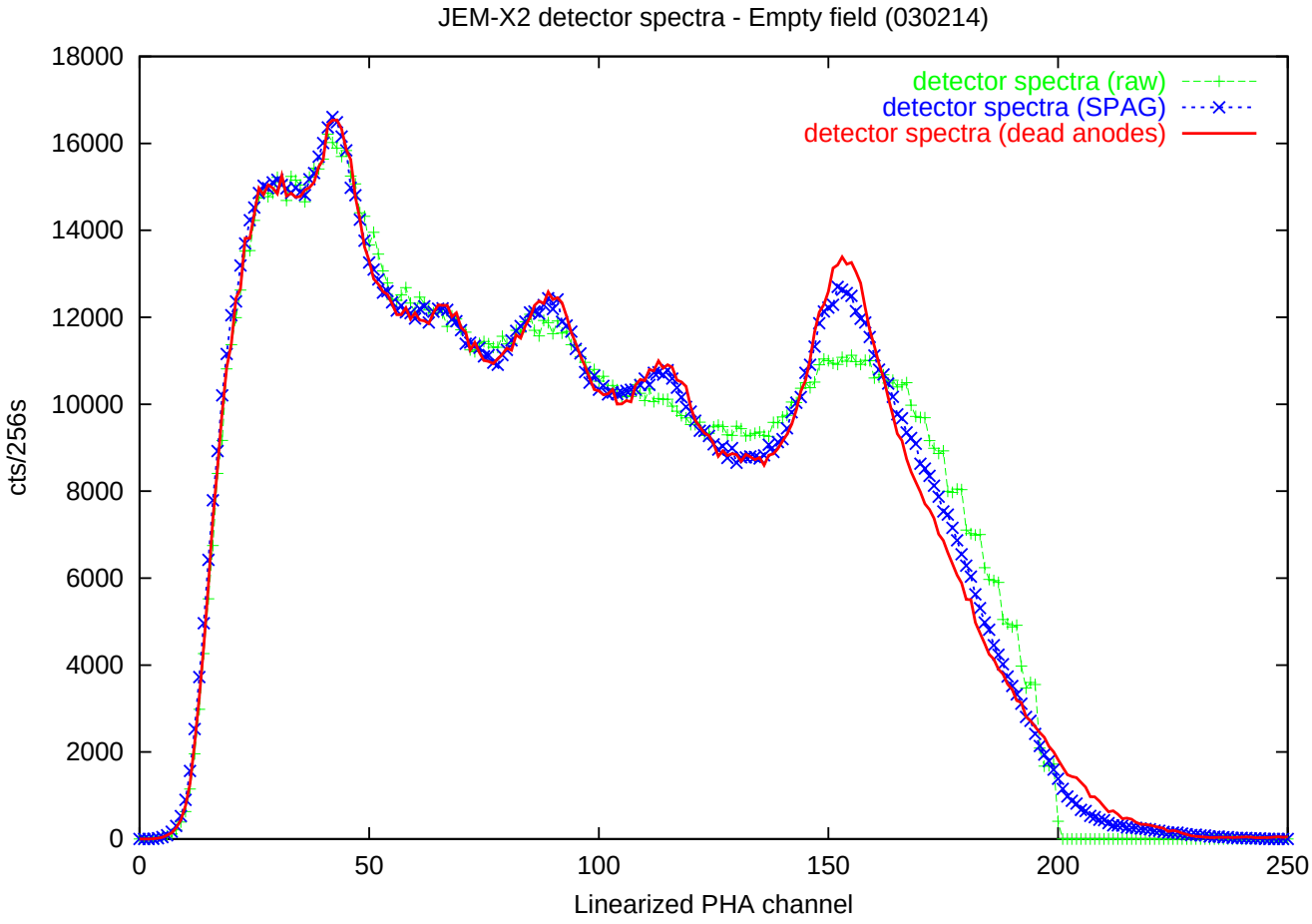

Figure 16: JEM-X2 spectra raw, corrected and dead anode-corrected data

N.B. The abcissa scale is customised linear channels for the offline analysis only

4.2 Deadtime correction

As with the gain corrections, deadtime correction has undergone a modest evolution since launch. Originally we had hoped to use the number of hardware triggers related to the number of software triggers in each 8 sec. housekeeping interval to determine the input deadtime, detection time lost due to reading data into the input buffer. However it has been determined that a significant fraction of hardware triggers are repeats of previous triggers. The method that is now used is to read all the different event classification counters in the housekeeping packets, and use these to determine: input deadtime, effective deadtime due to grey filter loss.

Currently flux and countrate corrections are performed on the basis of the input deadtime derived from the housekeeping data with 8 sec. time resolution, plus grey filter corrections based on the instrument status table (JMXi-INST-STA) grey filter values which have a time resolution equal to that of the rate at which the onboard software can change the grey filter. In the future buffer losses will also be included in the correction with 8 sec. resolution.

For detailed deadtime analysis on timescales shorter than 8 seconds users will have to do their own offline analysis. But the necessary data for this type of analysis are available.

4.3 Source detection

The source detection is based on a blind search for sources in the deconvolved image. The significance is determined as the peak size divided by the RMS value of the region just around the peak. The detection of a real source is ensured by demanding a certain limit for the significance. Simulations showed that a value of 12 would be adequate at least within 3 degrees from the pointing direction.

With real data this limit has to be set somewhat higher i.e. to about 14 due to non-uniform background in the detector and the loss of anodes.

4.4 Source Energy Spectrum Extraction

As an example of source extraction, figure 4.4 shows the image of the faint source EXO2030+375 which was detected by j_ima_src_find with a signal to noise ratio of 29.3, an average flux of 2.14 ± 0.05 counts/s. Vignetting (the decrease of collimator transmission with increasing off-axis angle) and increased noise in the partially coded field of view, both tend to limit the detector sensitivity at the edge of the field of view. Although the JEM-X field-of-view formally extend to 6.6 degrees off axis a more realistic limit seems to be 5 degrees.

The ISDC source extraction software was used to extract the spectra shown in figure 4.4. Each vertical error bar in the figure indicates a 1σ result, so it is clear that even for a fairly weak source we can make a 4–5 σ determination of the continuum. At low energies the effect of decreased detector sensitivity can also be seen (This observation was made prior to the latest update of the on-board parameters).

While these are reasonably good results for such a weak source it must be stressed that:

1. These are fairly preliminary results, using the first OSA software released by ISDC in April 2003. It can be expected that better results will be obtained by the use of better imaging techniques, improved vignetting corrections and by using the background handling software once it is working (see 'Future Work' below). It is hoped that all the improvements listed below will be implemented

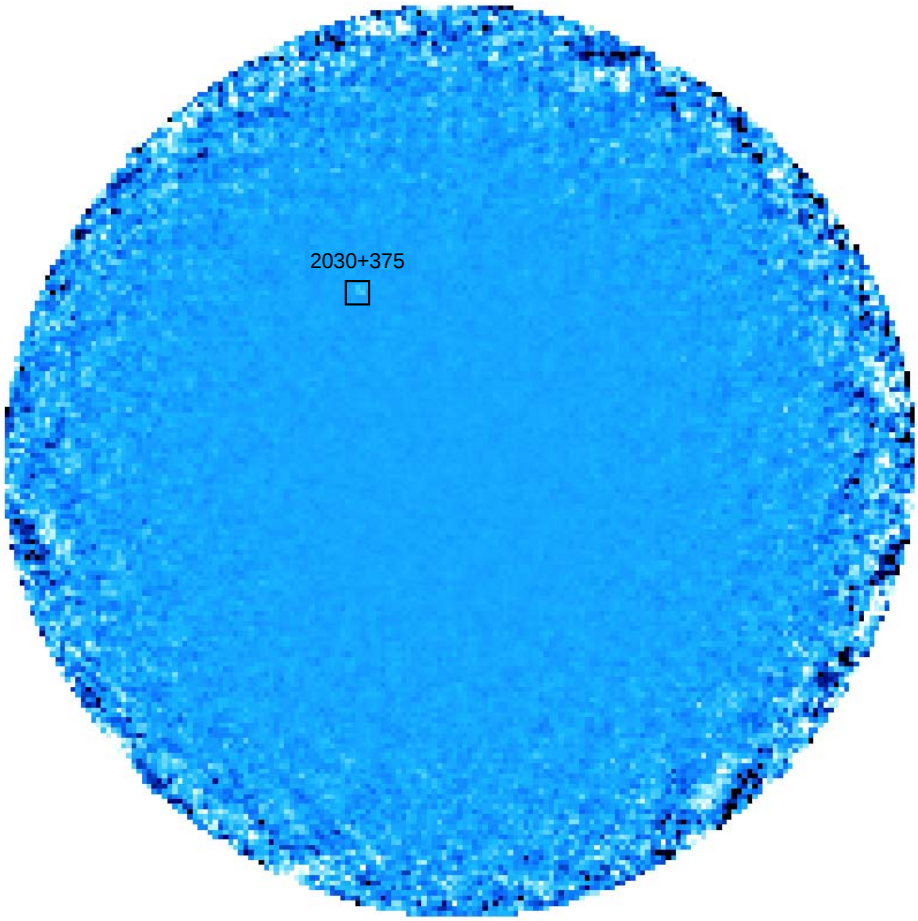

Figure 17: ISDC Image of source EXO2030+375 (Courtesy S. Martinez)

for the next OSA release in July-September 2003

2. The significance of the results, especially for faint sources, depends very strongly on where the source appears in the detector field of view. The results presented here are well within the fully coded field of view, but outside this area, the detector sensitivity is strongly curtailed not only by the collimator transmission and mask behaviour, but by our current vignetting procedure.

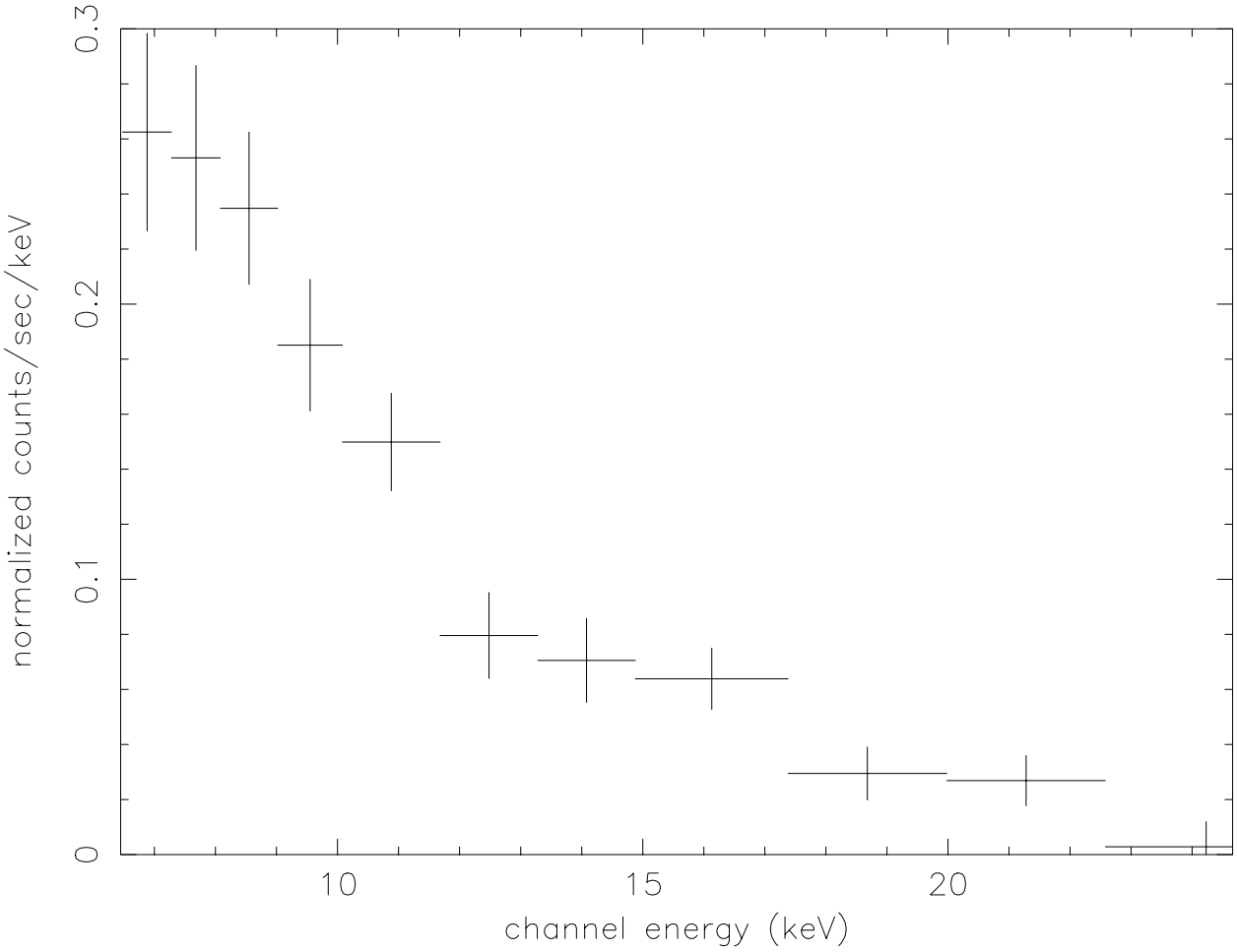

Figure 18: Spectrum of EXO2030+375 in range 6.9 to 24 KeV (Courtesy S. Martinez)

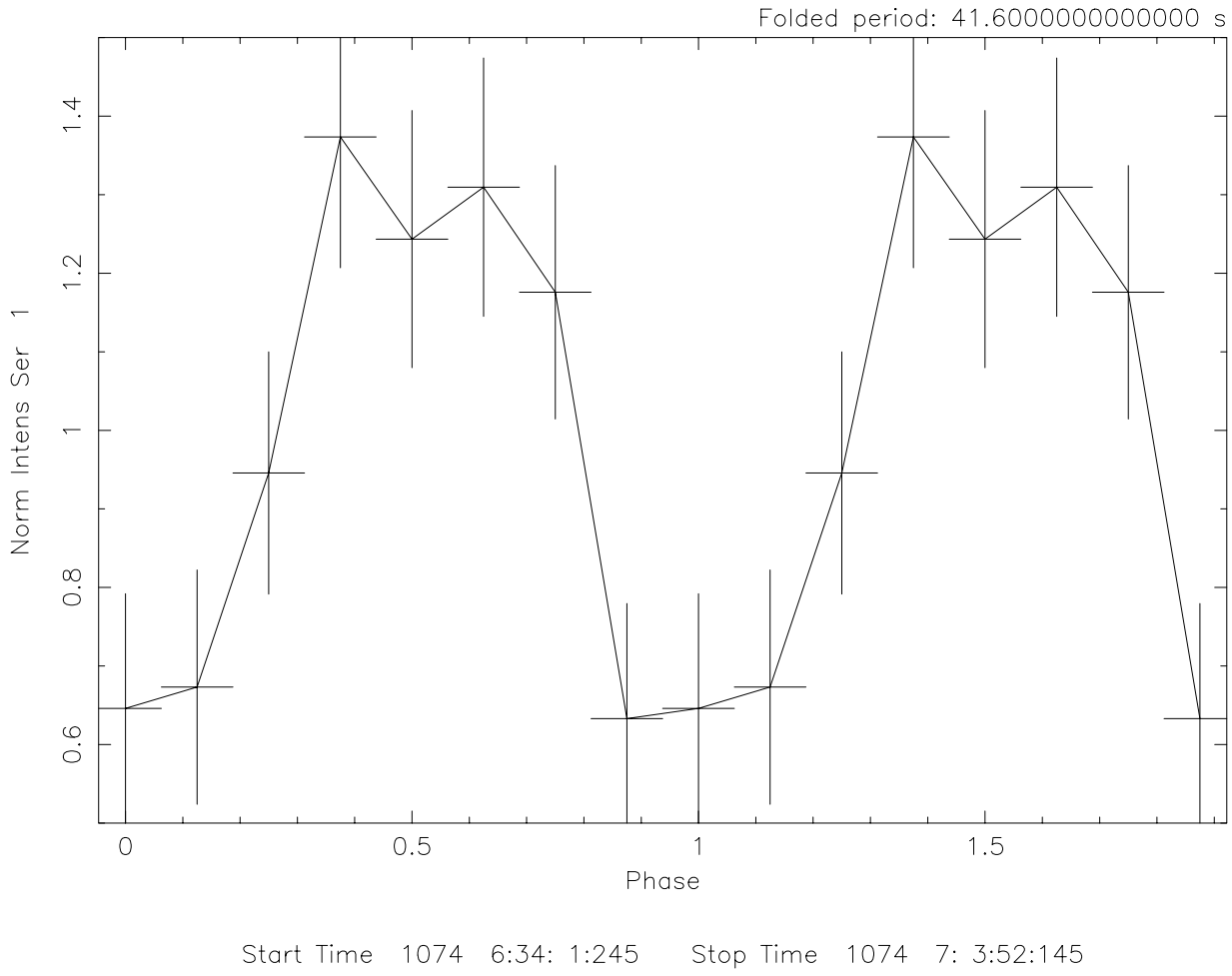

Figure 19: Pulse profile of EXO2030+375 (Courtesy S. Martinez)

4.5 Source Light Curve Extraction

Figures 4.5 shows the pulse shape of the faint source EXO2030+375 already discussed. The basis for this analysis was the lightcurve extracted by the ISDC software, which was then processed using the ftools efsearch and efold to find the best period (41.6 ± 0.1 sec.) and make the pulse profile. The best results were achieved using a bin length of 1.3 sec. All the comments that applied to the spectral analysis should be taken into account for this data also.

4.6 Conclusions

While much of the ISDC software has had to be changed since the launch to take into account the changing realities of the instrument performance (dead anodes; missing spectral lines for calibration; changes in high voltage and low energy discriminator settings; changes in electronic calibration; double hardware triggers etc.), the software that was recently released is both stable and capable of performing all the scientific processing required of it. The OSA user should be able to obtain, images, position and flux estimates, spectra and lightcurves from their data without too much trouble.

It is recognised however, that there is still room for improvement, and a list of currently planned future work is given below. Other more technical improvements to the software are also planned e.g. monitoring anode preformance automatically and making a history table of electronic calibration results.

4.7 Future work

Dead anode correction While a second layer is already available in the JMXi-SPAG-MOD tables for dead anode gain corrections, the tables of corrections are yet to be made and a small change must be made to the software component j_cor_gain to utilise this table slice for these corrections.

Buffer loss Currently buffer loss is not included in the 8 sec. time resolved deadtime corrections. This is a rare source of deadtime but when it occurs it can be quite large and we expect to add this correction within the next couple of weeks.

Refined imaging New imaging software is being developed to improve the sensitivity of the instrument for automatic source detection.

Background handling Determination of the amount of diffuse and instrument background counts is based on a catalogue of models of background spectra mapped onto the different areas of the detector. Until a good catalogue of background models has been created the background handling step of the processing cannot be performed in a way that improves the scientific results. Now that the majority of the software changes and configuration changes are complete the catalogue is being created from empty field observations. The background handling step of the scientific analysis is expected to be ready for use with the next OSA release in July/September 2003.

Vignetting Considerable variations in flux determinations are seen in the source detection results, and these have been traced back to the currently low resolution of the vignetting table, and uncertainty in source positions, both of which affect flux values very strongly. It is clear that the vignetting table is going to have to be redelivered with better resolution. Improved imaging techinques should help to decrease source position uncertainties.

Source positions The systematic 22" source position offset needs to be tracked down (possibly to the ISDC misalignment matrix) and dealt with.

Improved detector map Currently events can be rejected for further use in the science analysis based on bad detector gain determination or bad time correlation. It is planned to extend this mechanism to events coming from various 'bad' regions of the detector e.g. in the calibration spectra overspill areas; on known dead or unstable anodes; on known hotspots. To implement this the detector map JMXi-DETE-MOD will be improved to contain many different values than it currently does, to indicate different problems on various parts of the detector.

5 JEM-X calibration files at ISDC

5.1 Delivered files

5.1.1 Instrument model

The instrument description files are delivered in a single file as a DAL group. Due to the changes in the JEMX configuration so far five different instrument description files are required to cover the time period from launch up to the present date. When the calibration is fine tuned more time periods will be required.

The elements of the group are described in Table 3.

Table 3: Contents of JMXi-IMOD-GRP

DS name	Description	Status
JMXi-ATAL-MOD	Material constants	OK
JMXi-ATCU-MOD	Material constants	OK
JMXi-ATMO-MOD	Material constants	OK
JMXi-ATXE-MOD	Material constants	OK
JMXi-ATBE-MOD	Material constants	OK
JMXi-QEFF-MOD	Quantum efficiency	Low energy question
JMXi-MASK-MOD	Mask description	OK
JMXi-COLL-MOD	Collimator description	OK
JMXi-DETE-MOD	Detector description	Must be updated with dead anodes
JMXi-DPOS-MOD	Position accuracy in detector	OK
JMXi-BORE-MOD	Bore sight info	obsolete
JMXi-VIGN-MOD	Vignetting correction	OK
JMXi-FULB-MOD	Channel numbers	OK
JMXi-RESB-MOD	Channel numbers	OK
JMXi-SPCB-MOD	Channel numbers	OK
JMXi-CALB-MOD	Channel numbers	OK
JMXi-FBDS-MOD	Channel numbers	OK
JMXi-RBDS-MOD	Channel numbers	OK
JMXi-SBDS-MOD	Channel numbers	OK
JMXi-CORX-MOD	Position correction table	OK
JMXi-CORY-MOD	Position correction table	OK
JMXi-SPAG-MOD	Spatial gain correction	OK
JMXi-DEAD-MOD	Dead time corrections	OK
JMXi-DXBS-MOD	Diffuse X-ray Background in detector	not used
JMXi-ENRG-MOD	Energy values for response	OK
JMXi-ECAL-MOD	Electronic calibration	OK
JMXi-EFLT-MOD	Effect of electronic threshold	in progress

5.1.2 Response matrix

A response matrix with corresponding ARF (Ancillary Response Function) based on the ground calibration has been delivered.

The response matrix as such is the best possible since the change of the energy resolution due to the lower high voltage setting is very small.

The ARF needs an update since the lower voltage has implied that the electronic low threshold cuts into the events below 6 keV. The estimate of reliable values for this effect is still in progress.

However, even without buffer loss included, we are confident that the wide variation we see in flux determination is due almost entirely to vignetting uncertainties and not to any problems with the deadtime correction. Once buffer loss is in place we believe that this correction will be done as well as it can within the limits of the time resolution of the housekeeping.

6 JEM-X Operations

6.1 Operational Performance

During the first months of INTEGRAL operations it has been found that the entry into the radiation belts occurs at higher altitudes than expected. sometimes at altitudes in excess of 80 000 km, compared to the pre-launch assumed altitude of 40000 km.

It was also found that JEM-X were even more sensitive to the low energy electrons in the outer radiation belts than the IREM monitor - not the least because a build-in scaling of the IREM counts in the Broadcast packet prevented the payload instruments from receiving the low significance bits of the IREM scalers. This problem has hopefully now been solved by a patch to the IREM on-board software.

The grey filter logic has proven to work well under all conditions.

JEM-X may be considered fully operable according to the current flight operations procedures.

6.2 Telemetry Requirements

The telemetry allocation for JEM-X is currently 8 packets for JEM-X2 and 1 packet for the dormant JEM-X1 per 8 s polling cycle. The 8 packets/cycle seems to be adequate for almost all observations. JEM-X has a buffering capability of about 60000 events on-board, and this makes the instrument capable of handling short duration bursts without loosing data.

Additionally, JEM-X has implemented a dynamic grey filtering logic on-board, which randomly rejects events at the entry to the computer in case the memory is more than half filled. This feature allows for a gradual increase or decrease in the event rate as the need arises, and this technique minimizes the potential effects on timing analyses arizing from the on-board grey filter rejection.

We recommend that when JEM-X1 is reactivated it is also given 8 packets/cycle in telemetry allocation. Considering the present scarcity of the telemetry resource, this should not happen before the telemetry bandwidth for INTEGRAL as a whole has been upgraded.

6.3 Operations with two JEM-X units?

At present only one JEM-X is active, the other instrument is dormant - the computer and the electronics is working but the detector high voltage is off.

JEM-X1 has been kept in the dormant state since the end of December, although it was temporarily revived for few weeks during the Crab calibrations. The instrument is therefore calibrated and ready to start observations.

The Crab calibrations were performed with JEM-X1 operating at a lower gas gain than JEM-X2, this is expected to reduce the rate of anode losses - in fact none have been seen in 7 weeks of operations at the current voltage setting since the beginning of December.

We recommend to start JEM-X1 operations again - at this reduced voltage - as soon as the telemetry situation improves.

Operating with two JEM-X units in parallel, will be a great help when detecting and verifying transients and bursts. The masks of the two units are oriented differently and artefacts are therefore normally not overlapping.

Operating with two JEM-X units will also help to recover the loss in sensitivity from which JEM-X currently suffer.

The rate of anode loss is sufficiently low that the integrated exposure operating with two JEM-X units in parallel significantly exceeds the exposure obtainable with sequential operation - even for a mission extending well beyond 5 years. Also the damage rate is so low that the sensitivity evolution can be monitores along the way and decisions about modifications to the operations plan can be made as the mission progresses.

7 Conclusions

The commissioning and performance verification of the two JEM-X instruments on INTEGRAL has been carried out. The operability has been verified and the spectral and spatial resolution has been found to be fully consistent with the values given in the Science Performance Report.

The good source localization capabilities exceeds the requirements, and can be applied to identification work, a recent example is the INTEGRAL source IGR J17464-3213, which were found in the analysis and communicated via ATEL. Soon thereafter a potential radio counterpart was found by VLA within the IBIS error circle which had a 2 arcminute radius (IAUC # 8105). Subsequent JEM-X observations have confirmed the consistency of the VLA source with the INTEGRAL hard X-ray source. This is illustrated in figure 7 which shows the clustering of 183 independent JEM-X detections of this source around a position near the radio position. These data are the result of an offline analysis for which the instrument misaligment matrix clearly also needs some additional fine tuning. The centroid of the JEM-X position is about 25" from the VLA position, the RMS scatter on the JEM-X positions is 14".

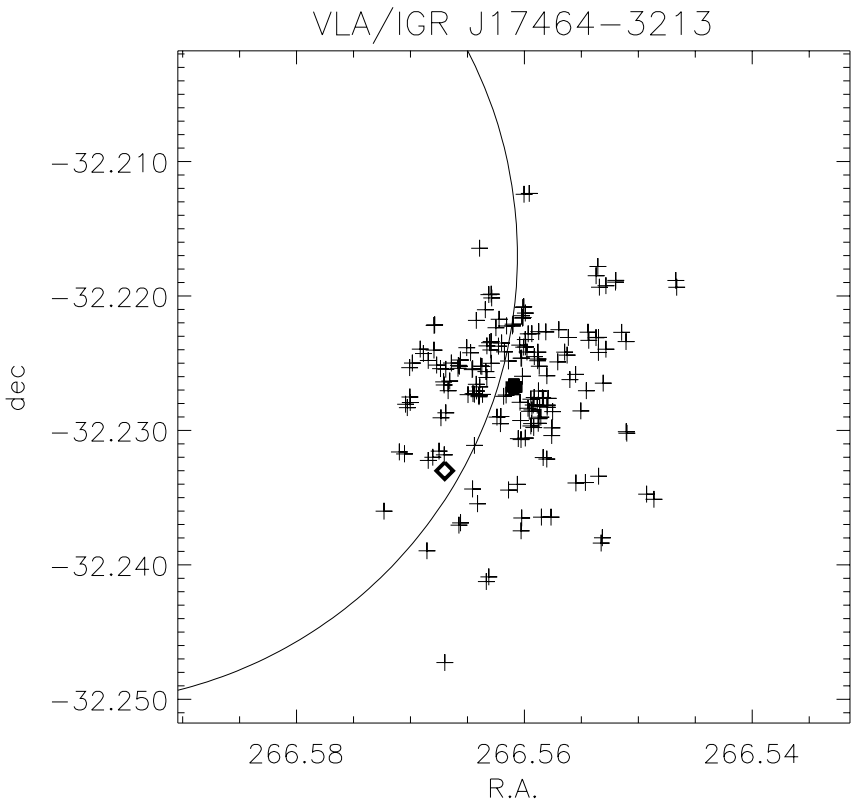

Figure 20: JEM-X localizations of the INTEGRAL source IGR J17464-3213. The circle segment is part of the original IBIS error circle, the diamond is the suggested radio counterpart, and the bold cross is the centroid of the JEM-X localizations. The JEM-X misalignment matrix is not yet final, so the discrepancy between the radio position and the JEM-X position is not significant.

The problems with the microstrip anodes have forced us to reduce the operating voltage and therefore the gas gain of the detectors.

With the lower gas gain our energy range have been reduced slightly, the lower threshold (50% efficiency point) has moved up from 3.5 keV to 4.2 keV.

Taken together, the higher background and operation with only one JEM-X will, at least for the first part of the mission, lead to a reduction of the JEM-X sensitivity by about a factor two compared to the values predicted before launch. To partially recover this loss it is recommended to reactivate the second JEM-X unit as soon as the planned increase in the INTEGRAL telemetry rate will allow this.

8 Appendix

8.1 Continuum sensitivity for source with known position

Compared to the results in the SPR Issue 4 revision 1 (June 2002) the changed detector properties as well as in the background lead to new sensitivity figures. The lowering of the gain implies that the low energy threshold is determined by the electronics rather that the absorption of the Be-window. For these calculation a revised quantum efficiency takes this into account.

The formulae are repeated here for clarity and factors have been introduced to describe the new performances.

The expressions are based on the assumption that the source is a point source located on the satellite pointing axis alone in the FOV and that in the image reconstruction (such as back-projection) only the part of the detector that can actually "see" the source contributes with background.

8.1.1 Continuum detection sensitivity

The fractional loss due to the degraded anodes is given by the factor λ_a, the fractional loss due to detector dead time by λ_d, and the loss due to the finite detector resolution is λ_p.

$$N_S = t_{mask}\, A(1-\lambda_a)\, q\, t_{obs}\, F_{Cont}\, \Delta E(1-\lambda_p)(1-\lambda_d) \quad (1)$$

$$N_B = t_{mask}\, B_{instr}\, A(1-\lambda_a)\, t_{obs}\, \Delta E \;+\; t_{mask}^2\, B_{DXB}\, q\, A(1-\lambda_a)\, t_{obs}\, \Delta E(1-\lambda_d) \quad (2)$$

$$n_\sigma = \frac{N_S}{\sqrt{N_B}} \quad (3)$$

$$F_{Cont} = \frac{n_\sigma}{q(1-\lambda_p)(1-\lambda_d)} \sqrt{\frac{B_{instr} \;+\; t_{mask}\, B_{DXB}\, q(1-\lambda_d)}{t_{mask}\, A(1-\lambda_a)\, t_{obs}\, \Delta E}} \quad (4)$$

N_S is the number of source source counts in the energy interval ΔE. A is the sensitive detector area, q the quantum efficiency (energy dependent) and t_{obs} the observation (exposure) time. F_{Cont} is the continuum flux in photons $\mathrm{cm}^{-2}\,\mathrm{s}^{-1}\,\mathrm{keV}^{-1}$. In Eq. 2 N_B is the number of background counts. The background can be split into two parts: The instrument background, B_{instr}, that is not influenced by the coded mask, and the Diffuse X-ray Background, B_{DXB}, that goes through the mask. B_{DXB} is the intensity disregarding mask and detector efficiency. Using t_{mask} as a factor in front of the parenthesis is based on the assumption that the analysis only involves the counts that could have an origin at the source. Otherwise the background will be increased with a factor of $1/t_{mask}$ and the limiting flux be increased with $1/\sqrt{t_{mask}}$.

The use of the expression in Eq. 3 is justified for long observation times where $N_B \gg 10$ which is certainly fulfilled for the value used: $t_{obs} = 10^5$s.

The table below is similar to the one given in the SPR Issue 4 Revision 1 p. 30 exept that the revised quantum efficiency has been used.

Energy keV	ΔE keV	$\bar{q}$	B_{instr} cts cm^{-2} s^{-1} keV^{-1}	B_{DXB} phot cm^{-2} s^{-1} keV^{-1}	F_{Cont} photons cm^{-2} s^{-1} keV^{-1}
6	6 (3 - 9)	0.48	1.0×10^{-3}	9.5×10^{-3}	2.4×10^{-5}
30	30 (15 - 45)	0.41	1.0×10^{-3}	9.0×10^{-4}	9.0×10^{-6}

$\bar{q}$ is the quantum efficiency averaged over the energy interval

Results at 6 keV and both JEM–X instruments				
λ_a	λ_d	λ_p	B_{instr} cts cm^{-2} s^{-1} keV^{-1}	F_{Cont} photons cm^{-2} s^{-1} keV^{-1}
0.08	0	0	1.0×10^{-3}	2.5×10^{-5}
0	0.18	0	1.0×10^{-3}	2.8×10^{-5}
0	0	0.40	1.0×10^{-3}	4.0×10^{-5}
0.08	0.18	0.40	1.0×10^{-3}	4.8×10^{-5}
Results at 6 keV and one JEM–X instrument				
0.08	0.18	0.20	1.0×10^{-3}	6.8×10^{-5}

Results at 30 keV and both JEM–X instruments				
λ_a	λ_d	λ_p	B_{instr} cts cm^{-2} s^{-1} keV^{-1}	F_{Cont} photons cm^{-2} s^{-1} keV^{-1}
0.08	0	0	1.0×10^{-3}	9.4×10^{-6}
0	0.18	0	1.0×10^{-3}	1.1×10^{-5}
0	0	0.20	1.0×10^{-3}	1.1×10^{-5}
0.08	0.18	0.20	1.0×10^{-3}	1.4×10^{-5}
Results at 30 keV and one JEM–X instrument				
0.08	0.18	0.20	1.0×10^{-3}	2.0×10^{-5}

8.2 Line detection sensitivity in known source

$$N_S = t_{mask}\, A(1-\lambda_a)\, q\, t_{obs}\, F_{Line}(1-\lambda_p)(1-\lambda_d) \quad (5)$$

$$N_B = t_{mask}\, B_{instr}\, A(1-\lambda_a)\, t_{obs}\, \Delta E_{FWHM} + t_{mask}^2\, B_{DXB}\, q\, A(1-\lambda_a)\, t_{obs}\, \Delta E_{FWHM}\, (1-\lambda_d) \quad (6)$$

$$n_\sigma = \frac{N_S}{\sqrt{N_B}} \quad (7)$$

$$F_{Line} = \frac{n_\sigma}{q(1-\lambda_p)(1-\lambda_d)} \sqrt{\frac{(B_{instr} + t_{mask}\, B_{DXB}\, q)\, \Delta E_{FWHM}}{t_{mask}\, A(1-\lambda_a)\, t_{obs}}} \quad (8)$$

The line flux, F_{Line} is given in photons cm^{-2} s^{-1}. The energy interval, ΔE_{FWHM}, is now as small as possible i.e. roughly the FWHM of the detector energy resolution. It is further assumed that the continuum flux from the source is insignificant with respect to the background.

Energy keV	ΔE keV	q	B_{instr} cts cm^{-2} s^{-1} keV^{-1}	B_{DXB} phot cm^{-2} s^{-1} keV^{-1}	F_{Line} photons cm^{-2} s^{-1}
6	1.0	0.78	1.0×10^{-3}	8.0×10^{-3}	4.3×10^{-5}
30	2.2	0.25	1.0×10^{-3}	7.8×10^{-4}	1.2×10^{-4}

Results at 6 keV and both JEM–X instruments				
λ_a	λ_d	λ_p	B_{instr} cts cm^{-2} s^{-1} keV^{-1}	F_{Line} photons cm^{-2} s^{-1}
0.08	0	0	1.0×10^{-3}	4.5×10^{-5}
0	0.18	0	1.0×10^{-3}	5.0×10^{-5}
0	0	0.40	1.0×10^{-3}	7.1×10^{-5}
0.08	0.18	0.40	1.0×10^{-3}	8.5×10^{-5}
Results at 6 keV and one JEM–X instrument				
0.08	0.18	0.40	1.0×10^{-3}	1.2×10^{-4}

Results at 30 keV and both JEM–X instruments				
λ_a	λ_d	λ_p	B_{instr} cts cm^{-2} s^{-1} keV^{-1}	F_{Line} photons cm^{-2} s^{-1}
0.08	0	0	1.0×10^{-3}	1.2×10^{-4}
0	0.18	0	1.0×10^{-3}	1.4×10^{-4}
0	0	0.20	1.0×10^{-3}	1.5×10^{-4}
0.08	0.18	0.20	1.0×10^{-3}	1.9×10^{-4}
Results at 30 keV and one JEM–X instrument				
0.08	0.18	0.20	1.0×10^{-3}	2.4×10^{-4}

JEM-X microstrip detectors

In-flight evolution

Technical note JEMX-DSRI-2003-1

N, Lund, C.B. Jørgensen, S. Brandt, J. Chevenez, C.A.Oxborrow
and N.J.Westergaard
2003-04-10

1) Recapitulation of the microstrip anode loss problem

Prior to the launch of INTEGRAL it was planned to operate both JEM-X units at a gas gain of 1500.

JEM-X1 was activated on October 27, the desired gas gain was reached at a HV setting of 900 V, corresponding to the pre-launch prediction.

JEM-X2 was activated on October 29, the desired gas gain was reached at a HV setting of 880 V, 10 V below the pre-launch prediction (the gas gain in JEM-X2 had always been slightly higher than in JEM-X1 for the same voltage).

On November 7 it was realized that the microstrip anodes were being rapidly eroded and both JEM-X units were switched off.

By that time 9 anodes had been lost in JEM-X1 during 11 days of operation and 12 anodes lost in JEM-X2 during 9 days of operation. (Figures 1 and 2 illustrates graphically the anode loss history).

JEM-X1 was reactivated on November 9 with a HV setting of 820 V. This corresponded to a gas gain of 450 (30 % of nominal).

JEM-X2 was reactivated on November 12 with a HV setting of 800 V and a gas gain of 450 (30 % of nominal).

During the next month a further 3 anodes were lost in JEM-X1, no further damage was seen in JEM-X2. As a consequence, it was decided that JEM-X1 should be placed in a dormant mode when the PV phase was completed, and further, that the JEM-X1 HV value should be reduced by 2 steps (20 V).

This was implemented on December 11, the JEM-X1 voltage was reduced to 800 V corresponding to a gas gain of 350 (23 % of nominal).

JEM-X1 was kept in a dormant mode with the HV off between December 29, 2002 and February 7. 2003. It was operated at 800 V during the Crab calibration (February 7-28), and remains in the dormant mode after February 28.

Now, at the beginning of April 2003 we have lost 4 anodes in JEM-X2 in the 4.5 months of continous operation at 800 V since November 12, 2002. We have seen no further anode losses in JEM-X1 in its 6 weeks of intermittent operation at 800 V since the beginning of December.

It appears that the current anode loss rate is one anode per month in JEM-X2 and maybe less than that in JEM-X1. At the current loss rate the effective area of JEM-X2 is reduced by about 6% per year. This rate is unpleasant, but not alarming and it is recommended that JEM-X2 is operated at the about the current gas gain at least until the next Crab calibration opportunity in July-August.

It would be an advantage scientifically to reactivate JEM-X1. However, due to the current lack of understanding of the gain evolution of the microstrip detectors (see below) and the shortage of telemetry, we suggest to leave JEM-X1 in the dormant mode until after the INTEGRAL Mission Performance Review and the implementation of the telemetry system upgrade.

Tables I summarizes the current dead-anode situation for the two JEM-X units.

2) Microstrip gain evolution.

It has been realized that both JEM-X units exhibit a steady increase in gas gain with time when operating at a constant voltage setting.

The effect is most pronounced in JEM-X2, but also apparent in JEM-X1. (Figure 3 and 4). It can also be noted that the rate of gain change has decreased in both JEM-X units, most noticeable in JEM-X1.

Figure 3 and 4 also shows that the calibration sources are reliable indicators for the time evolution of the gas gain for the detector as a whole, the global gain is measured using the Xenon fluorescense peak recorded all across the detector

Apparently the gas gain is changing more rapidly when the detector is active than when it is off. However, this conclusion is not absolutely certain, because the current gain drift in JEM-X1 is anyway very small.

Figure 5 and 6 shows a more detailed analysis of the gain evolution of JEM-X2, here the temperature effects on the gain have been removed. Figure 6 shows that the rate of gain change is decreasing, from about 14 % per month initially to about 6 % per month at present.

Using our housekeeping data we have checked the stability of the high-voltage power supplies and they seem to be very stable in both JEM-X units; the observed variations of the output voltages corresponds to gain changes at the percent level over first six months of operation.

We have also checked the detector pressure sensors. Unfortunately they only measures the pressure in crude steps (about 2.5% per step). There are in fact indications that we may have a gas leak from JEM-X2, maybe about 2.5% per year, whereas the gas pressure in JEM-X1 appears constant within the uncertainties. Indeed, if we have lost 1% of the gas in JEM-X2 during the first 5 months of the mission, then this may account for some 15% of the gain

increase, and this may at least partially explain the observed difference between JEM-X1 and JEM-X2

We have considered whether the effect could be due to radiation damage of the microstrip plates or the voltage divider circuits. But the different behaviour of JEM-X1 and -2 speaks against this.

For the time being we consider a small gas leak in JEM-X2 plus a change in the gas composition as the most likely explanation. This could be a partial removal of the methane quench gas due to polymerization or liberation of a new gas component with "Penning"-action. Both effects are likely to depend on the duty cycle of detector usage - thus the higher change rate in JEM-X2 is a natural consequence of its continous usage. However, given the almost constant detector pressure we consider it rather unlikely that the methane concentration by itself has changed enough to explain the observed change in gain.

We do not consider the gain change (or the gas leak) as a threat to the lifetime of the detector. We intend to adjust the high voltage so as to keep the gas gain close to value at which the Crab calibrations were performed. We will monitor the gain evolution continously for the future and take action, should new trends become apparent.

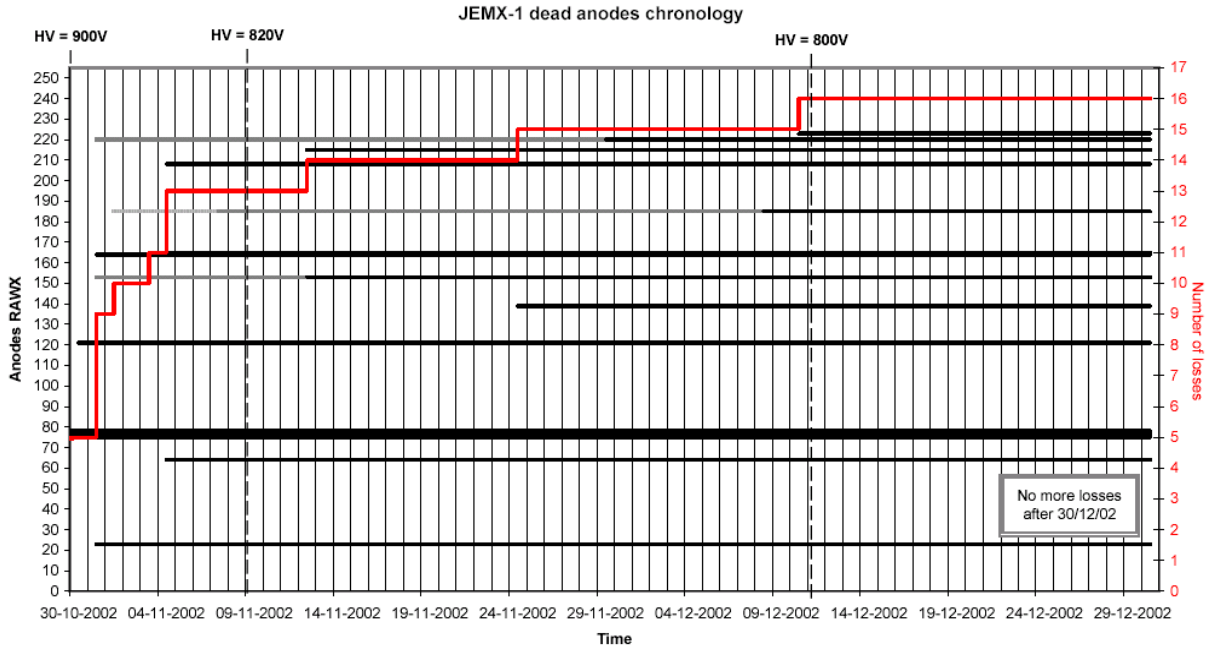

Figur 1 Time evolution of anode losses in JEM-X1

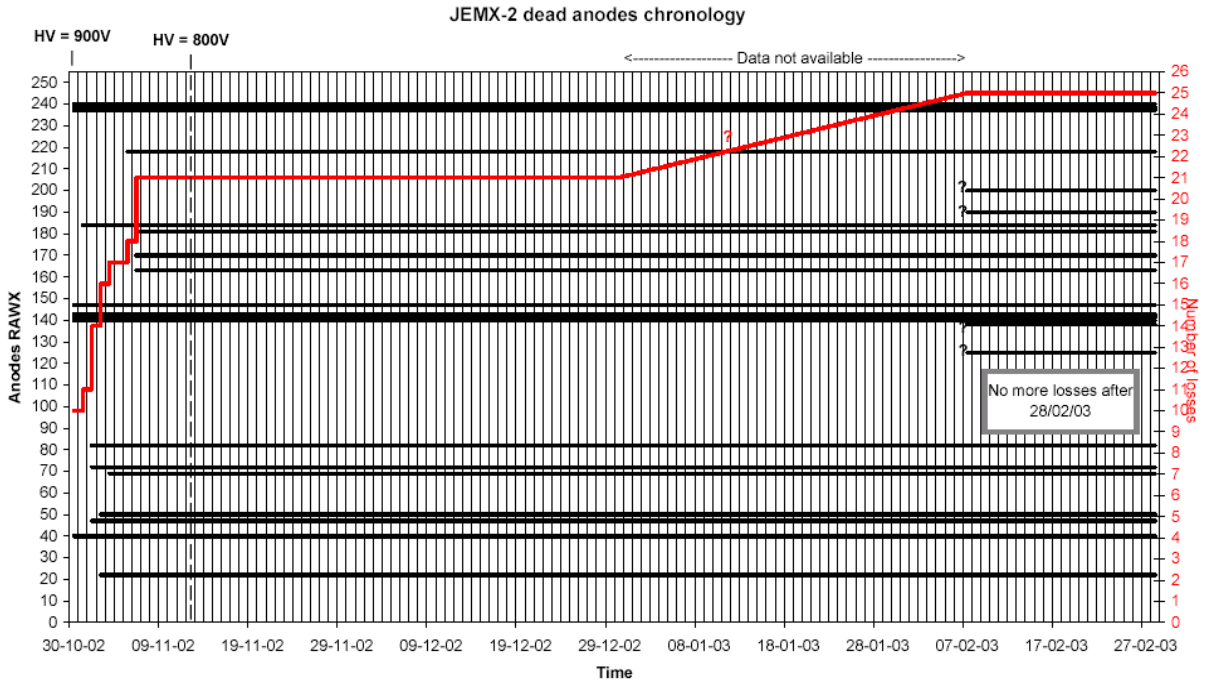

Figur 2 Time evolution of anode losses in JEM-X2

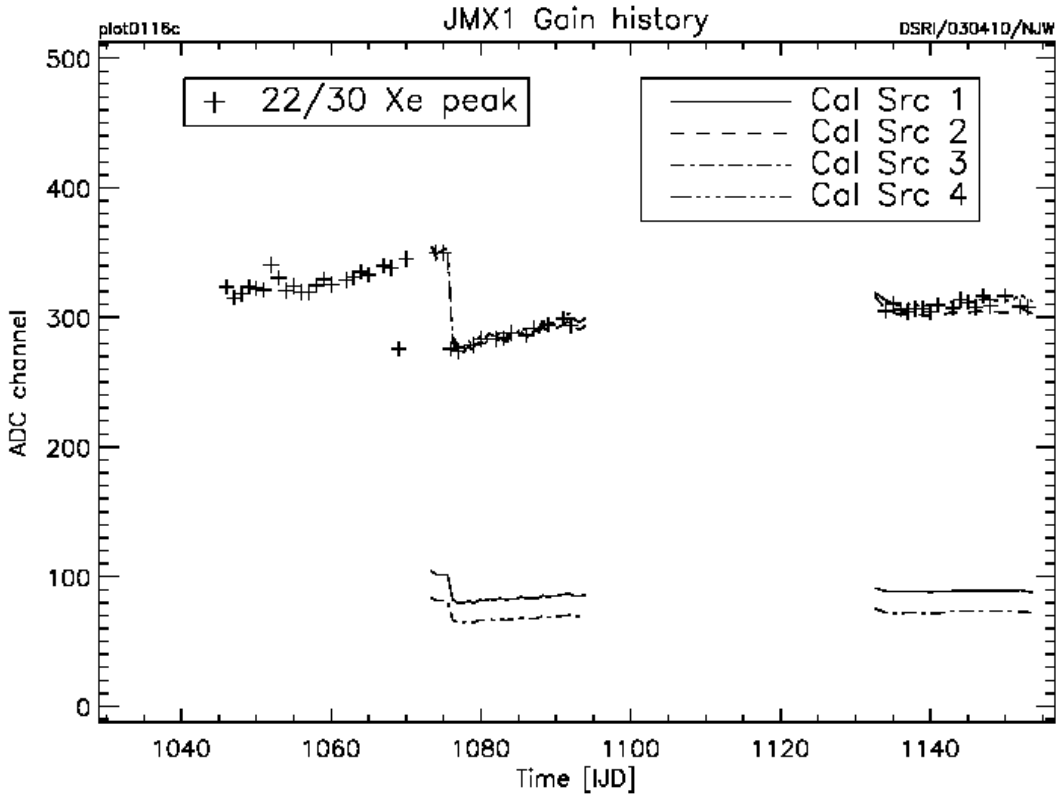

Figur 3 Gain evolution in JEM-X1. Note the perfect correspondence between the Xenon curve in this figure (the crosses) and the curves for the two calibration sources #2 and #4. Calibration sources #1 and #3 are Fe55 sources emitting at 6 keV, #2 and #4 are Cd109 emitting at 22 keV.

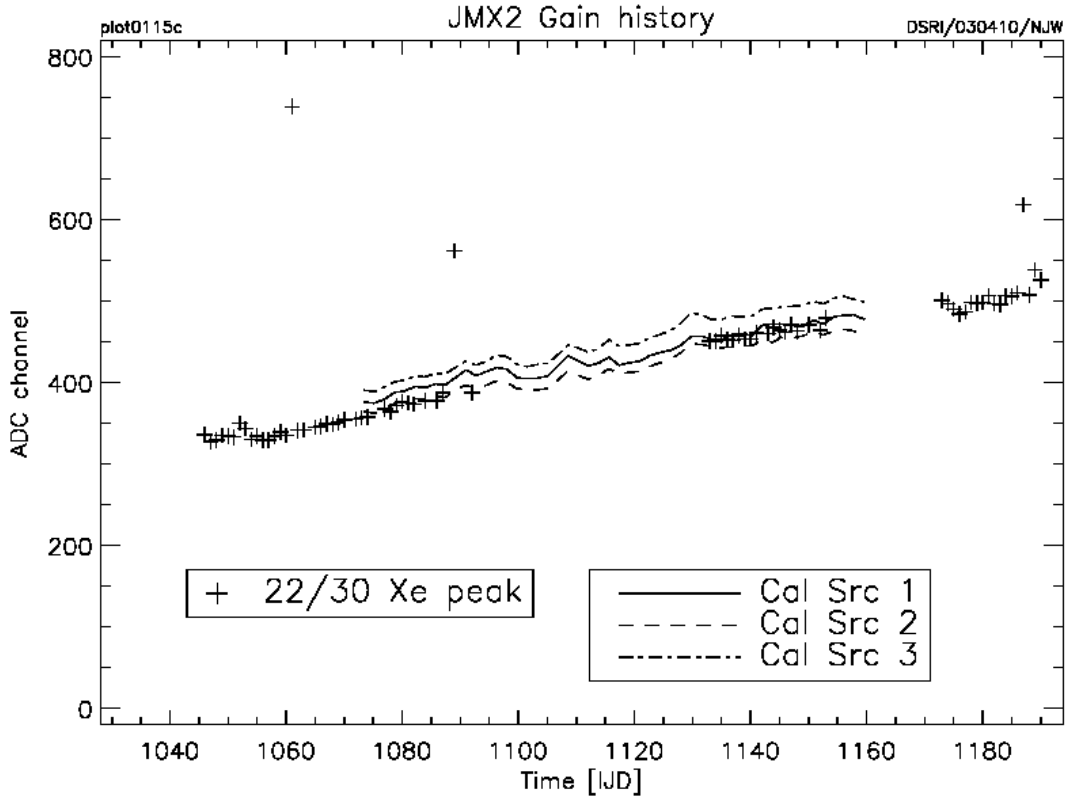

Figur 4 Gain evolution in JEM-X2

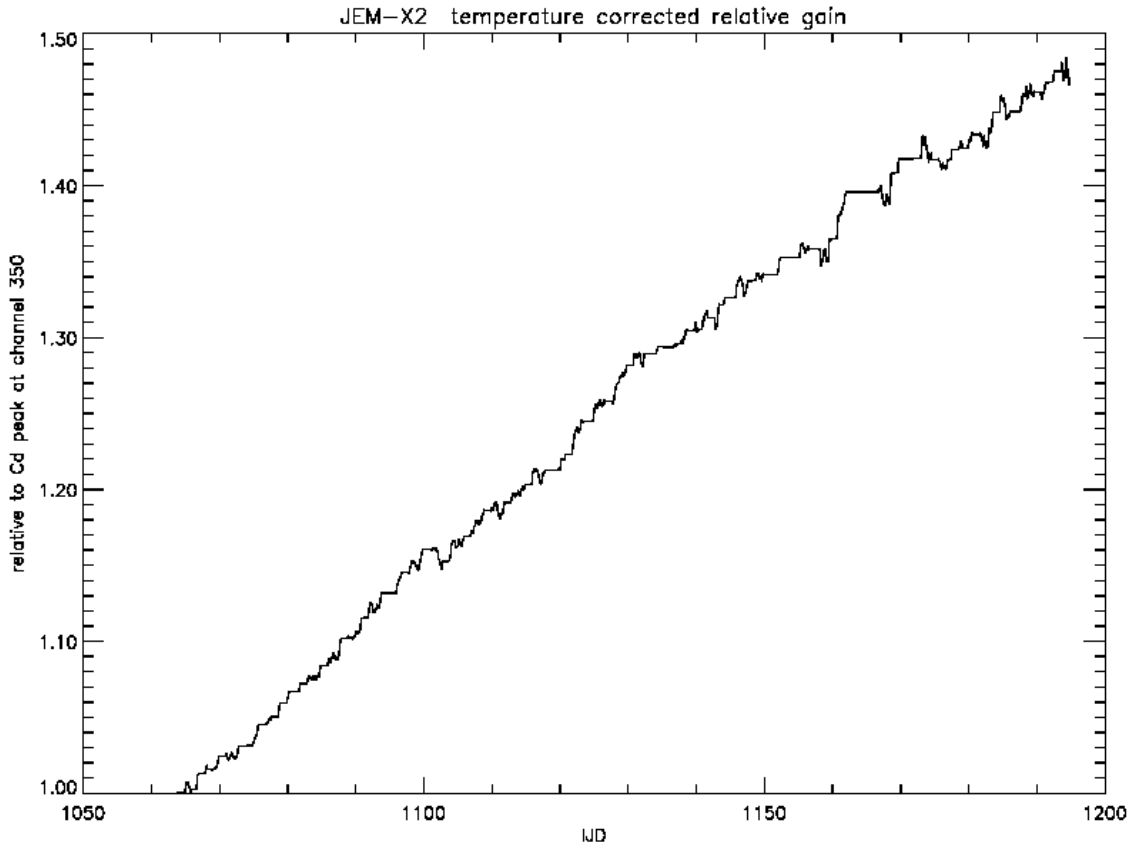

Figur 5 JEM-X2 gain evolution, temperature corrected

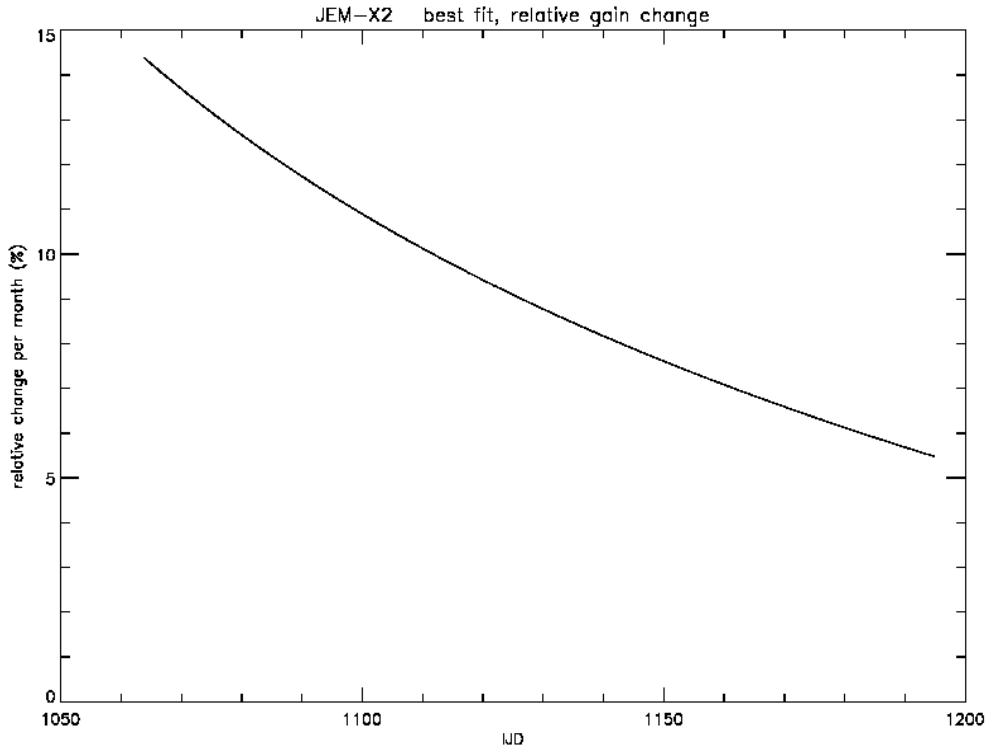

Figur 6 Fit to the gain evolution in JEM-X2

Dates	JEMX-1 Dead anodes	JEMX-2 Dead anodes
Launch (17/10/02)	75-78	140-143 147 237-240
< 30/10/02	121	40
31/10/02	23, 153(1), 164, 220(1)	184
01-11-02	185(1)	47, 72, 82
02-11-02		22, 50
03-11-02	165	69
04-11-02	64, 208	
05-11-02		218
06-11-02		163, 170, 181
07-11-02	185(2)	
12-11-02	153(2), 215	
24/11/02	139	
29/11/02	220(2)	
08-12-02	185(3)	
10-12-02	223	
11/12/02 – 29/12/02		
30/12/02 – 07/02/03	Data not available	
	(off)	125, 138, 190, 200
07/02/03 – 28/02/03		
01/03/03 – 19/03/03	*(off)*	Data not available
20/03/04 – 09/04/03	*(off)*	
STATUS	4 dead anodes before launch 12 after launch 6 unstable 10 low	9 dead anodes before launch 16 after launch 3 unstable 12 low

JEMXs' dead anodes RAWX positions listed in chronological order.

185(3) indicates the "third"death of anode 185.

The low anodes are neighbours to dead anodes.